# A STUDY OF ATMOSPHERIC FRONTOGENESIS WITH THE PRIMITIVE EQUATIONS

Richard Reuben Hadfield

# United States
# Naval Postgraduate School


# THESIS

A STUDY OF ATMOSPHERIC FRONTOGENESIS
WITH THE PRIMITIVE EQUATIONS

by

Richard Reuben Hadfield

April 1970

# A Study of Atmospheric Frontogenesis with the Primitive Equations

by

Richard Reuben Hadfield
Lieutenant Commander, United States Navy
B.S., United States Merchant Marine Academy, 1958

Submitted in partial fulfillment of the
requirements for the degree of

MASTER OF SCIENCE IN METEOROLOGY

from the

NAVAL POSTGRADUATE SCHOOL
April 1970

## ABSTRACT

The deformation of an unstable baroclinic wave as a result of mean horizontal wind shear is studied with the use of a five-layer primitive equation model. Two basic wind profiles were tested: 1) uniform zonal flow, 2) jet type zonal flow. The jet profile produced a cold front and a warm front, with the warm front being the more intense. The uniform zonal flow produced a cold front. The cold fronts were produced by horizontal shearing deformation fields and the warm front was produced by horizontal stretching deformation fields. The formation of the warm front was also enhanced by strong horizontal convergence. The occlusion process was not observed in the experiments.

TABLE OF CONTENTS

## LIST OF FIGURES

## LIST OF SYMBOLS

| | |
|---|---|
| $C_p$ | Specific heat of air at constant pressure |
| f | Coriolis parameter |
| $f_o$ | Coriolis parameter at center of region ($45^o$ north) |
| g | Acceleration of gravity |
| i | Grid index in x (east-west) direction |
| j | Grid index in y (north-south) direction |
| k | Grid index in vertical (pressure) direction |
| L | Wavelength in x direction |
| p | Pressure (independent variable) |
| $p_o$ | 1000 mb |
| R | Gas constant of air |
| t | Time (independent variable) |
| T | Temperature |
| u | Velocity component in x direction |
| U | Initial disturbance velocity |
| v | Velocity component in y direction |
| w | dz/dt, vertical velocity component |
| W | Width of domain (north-south) |
| x,y | Independent space coordinates (east-west, north-south) |
| z | Height of constant pressure surface |
| $\beta_o$ | Derivative of coriolis parameter at center of region ($45^o$ north) |
| $\theta$ | Potential temperature |
| $\theta_o$ | Potential temperature at $p = p_o$, $288.16^oA$. |

$\bar{\theta}$ . . . . Average potential temperature in the vertical

$\rho$ . . . . Density of air

$\varkappa$ . . . . $R/C_p$

$\phi$ . . . . Geopotential

$\omega$ . . . . dp/dt, velocity component in vertical for x,y,p coordinate system

$\nabla$ . . . . Del operator (horizontal)

$\Delta p$ . . . . Finite difference in vertical (pressure)

$\Delta x$ . . . . Mesh length in x direction

$\Delta y$ . . . . Mesh length in y direction

ACKNOWLEDGEMENTS

The author wishes to thank Professor R. T. Williams for suggesting this study and for his patience, guidance and encouragement as thesis advisor. The author also wishes to extend his thanks to Professor R. J. Renard for reading the manuscript and making several useful suggestions. The Naval Postgraduate School Computer Facility provided time on its IBM 360 computer for the numerical integrations.

# I. INTRODUCTION

The concept of atmospheric fronts has been accepted for many years, yet at this time there is no mathematical theory which can explain the formation of a front. Williams [1967] has indicated that the basic problem is finding a process which can produce a small-scale motion field from one which initially contains only large-scale motions.

A number of studies have been conducted evaluating mechanisms which are contributing factors in the formation of a front from an initial large-scale baroclinic wave. Stretching deformation wind fields have been studied by Stone [1966] and Williams and Plotkin [1968], while shearing deformation wind fields have been studied by Arakawa [1962] and Williams [1967]. Stone [1969] indicates that these effects should be of about the same importance. Arakawa [1962], Edelmann [1963], Williams [1965, 1967] and Økland [1969] have studied atmospheric frontogenesis with vertical deformation fields with the general result that a realistic front is produced within a reasonable time period. Bushby and Timpson [1967] and Bushby [1969] have studied the dynamics of fronts and frontal rainfall with a primitive equation model utilizing real data with good results in a twenty-four hour forecast of rainfall.

The purpose of this study is to investigate the deformation of a unstable baroclinic wave as a result of horizontal shear in the mean wind field. The primitive equation model is basically the model used by Harrison [1969] with a slightly modified lower boundary condition and different geographical and theoretical areas of application.

## II. THE PRIMITIVE EQUATIONS

Consider the primitive equations in the following form, with heating, friction and curvature terms neglected and with the coriolis parameter a linear function of y:

$$\frac{\partial u}{\partial t} = - L(u) - \frac{\partial \phi}{\partial x} + fv, \tag{1}$$

$$\frac{\partial v}{\partial t} = - L(v) - \frac{\partial \phi}{\partial y} - fu, \tag{2}$$

$$\frac{\partial \theta}{\partial t} = - L(\theta), \tag{3}$$

$$\frac{\partial \omega}{\partial p} = - \left(\frac{\partial u}{\partial x} + \frac{\partial v}{\partial y}\right), \tag{4}$$

$$\frac{\partial \phi}{\partial p} = - C_p \theta \frac{\partial}{\partial p} \left(\frac{p}{p_o}\right)^{\kappa}, \tag{5}$$

where

$$L(s) = \frac{\partial}{\partial x} (us) + \frac{\partial}{\partial y} (vs) + \frac{\partial}{\partial p} (\omega s),$$

and $s = u, v, \theta.$

At $p = p_o$

$$\frac{\partial \phi}{\partial t} = - \frac{\partial}{\partial x} (u\phi) - \frac{\partial}{\partial y} (v\phi) + \phi \left(\frac{\partial u}{\partial x} + \frac{\partial v}{\partial y}\right) - \omega \frac{\partial \phi}{\partial p} . \tag{6}$$

Equations (1) through (3) and equation (6) are prognostic equations. Equations (1) and (2) are the momentum equations, equation (3) is the first law of thermodynamics and equation (6) is the lower boundary condition. The diagnostic equations (4) and (5) are the mass continuity and hydrostatic equations, respectively.

Equation (6), the lower boundary condition was obtained by setting $d\phi/dt = gw = 0$, which implies that $w = 0$ at the lowest level.

Phillips [1963] has shown that the error resulting from the neglect of vertical motion at the lowest level is very small.

## III. FINITE DIFFERENCES

Equations (1) through (6) were solved numerically by introducing finite differences in x, y, p and t. The space finite differences employed were a variation of a scheme constructed by Arakawa [1966] [also see Lilly, 1965]. The basic scheme is designed to conserve total energy and also to conserve the squares of u, v and $\theta$ with respect to the advection terms.

The vertical domain is divided into five layers with the arrangement of variables as shown in Fig. 1.

| mb | Variable | Level (k) |
|---|---|---|
| 0 | $\omega = 0$ | 10 |
| 100 | $u,v,\emptyset,\theta$ | 9 |
| 200 | | 8 |
| 300 | $u,v,\emptyset,\theta$ | 7 |
| 400 | | 6 |
| 500 | $u,v,\emptyset,\theta$ | 5 |
| 600 | | 4 |
| 700 | $u,v,\emptyset,\theta$ | 3 |
| 800 | | 2 |
| 900 | $u,v,\emptyset,\theta$ | 1 |
| 1000 | $u,v,\emptyset,\theta,\omega$ | 0 |

Fig. 1. Distribution of variables in the vertical.

The finite difference form of the L(s) operator can be written

$$L(s)_{i,j,k} = \Big[(u_{i+1,j,k} + u_{i,j,k})\,(s_{i+1,j,k} + s_{i,j,k}) - (u_{i,j,k} + u_{i-1,j,k})\,(s_{i,j,k} + s_{i-1,j,k})\Big]/4\Delta x + \Big[(v_{i,j+1,k} + v_{i,j,k})\,(s_{i,j+1,k} + s_{i,j,k}) - (v_{i,j,k} + v_{i,j-1,k})\,(s_{i,j,k} + s_{i,j-1,k})\Big]/4\Delta y + \Big[(\omega_{i,j,k+1})\,(s_{i,j,k+2} + s_{i,j,k}) - (\omega_{i,j,k-1})\,(s_{i,j,k} + s_{i,j,k-2})\Big]/2\Delta p.$$

The linear space derivatives are of the general form

$$\frac{\partial s}{\partial x} = (s_{i+1,j,k} - s_{i-1,j,k})/2\Delta x.$$

The hydrostatic equation (6) can be written in finite difference form following Lorenz [1960] as

$$\phi_{i,j,k+2} = \phi_{i,j,k} + \frac{(\theta_{i,j,k} + \theta_{i,j,k+2})}{2} C_p \left[\left(\frac{p_k}{p_o}\right)^{\kappa} - \left(\frac{p_{k+2}}{p_o}\right)^{\kappa}\right].$$

The form of vertical finite differences as specified in the L(s) operator and the hydrostatic equation were modified at level zero in the following manner.

1. $\theta$, u and v were linearly extrapolated from levels one and three to level zero.

2. $\partial\phi/\partial p$ at level zero was approximated by a one-sided difference.

Centered time differences were used throughout this study with the exception of the first time step which is forward. To prevent separation of solutions, the program was restarted every twelve hours with a forward time step.

The following basic steps were used in integrating the given system of equations.

1. The potential temperature and wind fields at the odd-numbered levels and the geopotential of the 1000 mb surface are prescribed initially.

2. The mass continuity equation is integrated in space from the highest level to the surface to obtain $\omega$.

3. The hydrostatic equation is integrated in space from the surface to the highest level to obtain $\emptyset$.

4. The momentum equations are integrated in time to obtain u and v at time $t + \Delta t$.

5. The first law of thermodynamics is integrated in time to obtain $\theta$ at time $t + \Delta t$.

6. The equation for the lower boundary condition is integrated in time to obtain the 1000 mb geopotential at time $t + \Delta t$.

7. Steps 2 through 6 are repeated for the number of time steps desired.

## IV. BOUNDARY CONDITIONS

The boundary conditions are specified in a manner that conserves mass and energy within the grid domain. At the northern and southern boundaries the normal component of velocity is zero and periodicity is enforced at the eastern and western boundaries. Fig. 2 illustrates the horizontal grid domain.

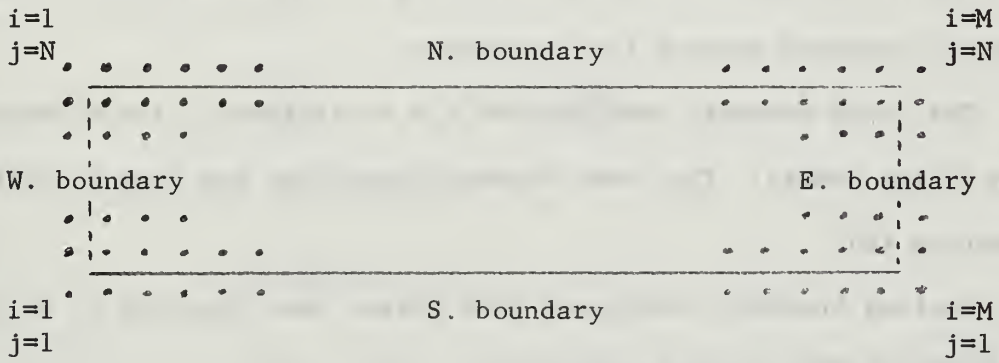


Fig. 2. Horizontal grid

The east-west boundary condition forces cyclic continuity on all parameters. This is accomplished by requiring the values in the two columns on the right to be the same as the values in the two columns on the left. This condition is specified by

$$s_{1,j} = s_{M-1,j} \qquad s_{2,j} = s_{M,j},$$

where

$$s = u,v,\emptyset,\theta.$$

The north-south boundary condition allows flow along the boundary but does not allow flux across the boundary. This is accomplished by imposing the following condition on the v term of the advection operator,

$$v_{i,1} + v_{i,2} = 0 \qquad v_{i,N} + v_{i,N-1} = 0$$

or

$$v_{i,1} = - v_{i,2} \qquad v_{i,N} = - v_{i,N-1}.$$

The values of geopotential and potential temperature in the outer row are set equal to the value in the next interior row. This is specified by

$$s_{i,1} = s_{i,2} \qquad s_{i,N} = s_{i,N-1} \tag{7}$$

where

$$s = \phi, \theta.$$

As a result of v being set equal to zero between the two outer grid points along the northern and southern boundaries, values of u and $\omega$ are not required outside the boundaries.

The upper boundary condition of $\omega = 0$ eliminates flux through the top of the domain. The lower boundary condition has been specified in equation (6).

Various boundary conditions were tested (see Appendix A) before acceptance of the above method.

## V. INITIAL CONDITIONS

The initial fields of u, v and $\theta$ were specified in order to generate a baroclinic zonal current. A small amplitude disturbance in the geopotential field; which is independent of pressure, was superimposed on the basic zonal flow. The mean zonal current ($\bar{u}$) has the following forms;

1) jet profile

$$\bar{u} = \frac{\hat{\partial u}}{\partial p} (p - p_o) \sin^2 \left(\frac{\pi y}{W}\right)$$

2) uniform zonal profile

$$\bar{u} = \frac{\hat{\partial u}}{\partial p} (p - p_o)$$

where $\hat{\partial u}/\partial p$ is constant. The initial data fields were generated in the following steps.

1. The geopotential at $p = p_o$ was calculated from

$$\phi_o = f_o U \frac{L}{2\pi} \cos \left(\frac{2\pi x}{L}\right) \sin^2 \left(\frac{\pi y}{W}\right) \qquad (8)$$

2. The potential temperature fields were specified from

$$\theta = \frac{p \left(\frac{p_o}{p}\right)^{\kappa}}{R} \frac{\hat{\partial u}}{\partial p} J + \theta_o + \frac{\hat{\partial \theta}}{\partial p} (p - p_o),$$

where $\hat{\partial \theta}/\partial p$ is a constant.

For uniform zonal flow

$$J = f_o y + \beta_o y^2/2.$$

For jet flow

$$J = f_o y + \beta y^2/2$$

$$-f_o \left[\frac{y}{2} - \frac{W}{4\pi} \sin\left(\frac{2\pi y}{W}\right)\right]$$

$$-\frac{\beta_o}{2}\left[\frac{y^2}{2} - \frac{W^2}{4\pi^2}\cos\left(\frac{2\pi y}{W}\right) - \frac{yW}{2\pi}\sin\left(\frac{2\pi y}{W}\right)\right].$$

3. The hydrostatic equation was then solved for the geopotential at all required levels.

4. The initial wind fields were then calculated from the geopotential fields using the geostrophic approximation. Thus, the initial fields were in geostrophic balance at time zero.

The basic current is zero at the lowest level and increases at a rate of 5 mps/100 mb to a maximum of 45 mps at 100 mb. Therefore $\partial\bar{u}/\partial z$ decreases with increasing altitude which reduces the baroclinic instability in the upper layers. This approximates the effects of a tropopause on the dynamics.

The initial disturbance amplitude was 10 meters or .125 mb. The small initial amplitude was chosen to prevent the excitation of large amplitude gravity waves that occur since the initial wind field was geostrophic.

The value of $\partial\hat{\theta}/\partial p$ used was $-.376^{\circ}C$/mb. This value is approximately one-half the value determined by Gates [1960] for winter over the United States, but it has the advantage of forcing the fronts to develop more rapidly and thus to reduce the computer time required. The value used approximated the standard atmosphere quite well in the lower levels, see Table I, but is less stable than the standard atmosphere in the upper levels. The stratosphere is clearly not represented

by this temperature field, however the dynamical presence of the stratosphere is represented by $\bar{u}$.

| Pressure (mb) | Height (meters) | |
|---|---|---|
| | Jet | Standard Atmosphere |
| 100 | 15325 | 16210 |
| 300 | 9112 | 9160 |
| 500 | 5576 | 5570 |
| 700 | 3015 | 3010 |
| 900 | 988 | 990 |
| 1000 | 110 | 110 |

Table I. Average initial height of constant pressure surface.

The beta plane approximation was made, where the coriolis parameter is a linear function of y. The quantities $f_o$ and $\beta_o$ were computed at $45^o$ north latitude.

Various combinations of grid size, time step and wind profile were tested. Table II is a summation of these various experiments.

| Experiment | Δx (km) | Δy (km) | Wind Profile | | Domain Dimension | | Time Step (min) |
|---|---|---|---|---|---|---|---|
| | | | Jet | Uniform Zonal | L (km) | W (km) | |
| 1 | 200 | 200 | X | | 4000 | 4000 | 6 |
| 2 | 200 | 200 | | X | 4000 | 4000 | 6 |
| 3 | 100 | 100 | X | | 4000 | 4000 | 3 |
| 4 | 100 | 100 | | X | 4000 | 4000 | 3 |
| 5 | 200 | 100 | X | | 4000 | 2000 | 3 |
| 6 | 200 | 100 | | X | 4000 | 2000 | 3 |
| 7 | 200 | 400 | X | | 4000 | 8000 | 6 |
| 8 | 200 | 400 | | X | 4000 | 8000 | 6 |

Table II. Summary of experiments.

## VI. RESULTS

All experiments were conducted using the values of $\partial\hat{u}/\partial p$, $\partial\hat{\theta}/\partial p$ and initial disturbance amplitude as specified by equation (8) in the initial condition section of this paper. Table II gives a listing of the specific variations in each of the following experiments.

Experiment No. 1. This is the basic jet flow experiment with a grid size of 200 km in x and y. The initial 1000 mb height analysis is given in Fig. 3 and the initial height and potential temperature analysis for the 900 mb and 700 mb surfaces are given in Figs. 4 and 5. The growth of the systems from day one through day four at the 900 mb surface is given in Figs. 6 through 9. By the end of three days a cold front and a warm front have formed and the temperature gradients are large by the fourth day. Note that the warm front contains larger gradients than the cold front. Large convergence (not shown) is associated with the warm front. The 700 mb analysis of height and potential temperature for days three and four is given in Figs. 10 and 11. The cold and warm fronts have the proper tilt in the vertical, with a slope between 1/125 and 1/250, which is computed at day three and for both fronts. The growth of the surface pressure centers, divergence and vorticity at 900 mb is given in Table III. It should be noted in Table III the asymmetry between the maximum and minimum values of each quantity.

Experiment No. 2. This is the basic uniform zonal flow experiment with a grid size of 200 km in x and y. The initial 1000 mb height analysis is given by Fig. 3 and the initial height and potential

| DAY | 1000 mb centers (m) | | Divergence ($\times 10^{-6}$) | | Vorticity ($\times 10^{-5}$) | |
|---|---|---|---|---|---|---|
| | Low | High | Max | Min | Max | Min |
| Initial | 100 | 120 | .3 | -.3 | .7 | -.7 |
| 1 | 90 | 130 | 2.2 | -2.4 | 1.0 | -1.0 |
| 2 | 40 | 160 | 3.7 | -7.3 | 2.9 | -1.8 |
| 3 | -60 | 190 | 6.5 | -17.1 | 9.4 | -3.0 |
| 4 | -200 | 270 | 20.7 | -41.9 | 18.9 | -6.6 |

Table III. Experiment No. 1.

temperature fields for the 900 mb and 700 mb surfaces are given in Figs. 12 and 13. The growth of the systems from day one through day four at the 900 mb surface is given in Figs. 14 through 17. By day three a cold front has formed to the west of an apparent warm front. However there is a single vorticity maximum in the region and there is no evidence of a warm front at higher levels. The front appears to be an occlusion but it did not evolve from two separate fronts with associated vorticity maxima. It was also noted that in the northern region of the low there was a packing of potential temperature lines which somewhat resembles the warm front in the jet flow experiment. The 700 mb pressure analysis of height and potential temperature for days three and four are given in Figs. 18 and 19. The front tilts to the west in the vertical with a slope between 1/60 and 1/120 at day three. The growth of the surface pressure centers, divergence and vorticity at 900 mb is given in Table IV.

Experiment No. 3. This experiment is the same as experiment 1 except that the grid length was reduced to 100 km in x and y. The results are basically the same as in experiment 1, with the exception

| DAY | 1000 mb centers (m) | | Divergence ($\times 10^{-6}$) | | Vorticity ($\times 10^{-5}$) | |
|---|---|---|---|---|---|---|
| | Low | High | Max | Min | Max | Min |
| Initial | 100 | 120 | .3 | -.3 | .7 | -.7 |
| 1 | 80 | 140 | 2.4 | -3.8 | 1.0 | -.8 |
| 2 | 30 | 170 | 8.3 | -8.8 | 1.8 | -1.5 |
| 3 | -120 | 240 | 10.9 | -22.0 | 10.0 | -2.9 |
| 4 | -550 | 340 | 23.3 | -43.7 | 25.7 | -4.5 |

Table IV. Experiment No. 2.

that the growth of the systems is now slightly faster with a slightly larger vorticity. The 900 mb height and potential temperature analysis for days three and four are given in Figs. 20 and 21. Note that the temperature gradients are larger in this experiment at four days than in experiment 1. This indicates that the larger truncation error with the larger grid size inhibits the energy cascade to small scales.

Experiment No. 4. This experiment is the same as experiment 2 except that the grid size was reduced to 100 km in x and y. A front similar to the one in experiment 2 developed, but in addition, a gravity wave with a wavelength of approximately 188 km was superimposed on the height analysis. The gravity wave was initially observed at day two close to the north and south boundaries, and by day three had completely covered the domain. It was apparently excited by the large shear at the boundary as generated by equation (7).

Experiment No. 5. This experiment is the same as experiment 1 except that $\Delta y$ was reduced to 100 km and W was reduced to 2000 km. Cold and warm fronts developed within three days that were similar to

the ones generated in experiment 1. Superimposed on the long wave pattern was a very small amplitude gravity wave with a wavelength of approximately 188 km.

Experiment No. 6. This experiment is the same as experiment 2 except that $\Delta y$ was reduced to 100 km and W was reduced to 2000 km. The results are the same as in experiment 2, but in addition, a gravity wave of small amplitude and approximate wavelength of 188 km was superimposed on the long wave pattern.

Experiment No. 7. This experiment is the same as experiment 1 except that $\Delta y$ was increased to 400 km and W was increased to 8000 km. See Figs. 22 and 23 for day three 900 mb height and potential temperature analysis. By day three a cold and warm front, similar to the results of experiment 1, had formed with the disturbance being limited to the central region of the domain.

Experiment No. 8. This experiment is the same as experiment 2 except that $\Delta y$ was increased to 400 km and W was increased to 8000 km. Gravity wave propagation, with an approximate wavelength of 400 km, from the north and south boundaries was too strong to permit an evaluation of the long wave system.

In none of the experiments was there an indication of a front at 500 mb or above. All energy calculations (see Appendix B) indicated that the potential energy was three orders of magnitude greater than the kinetic energy and that there was a small energy sink in the system up to four days.

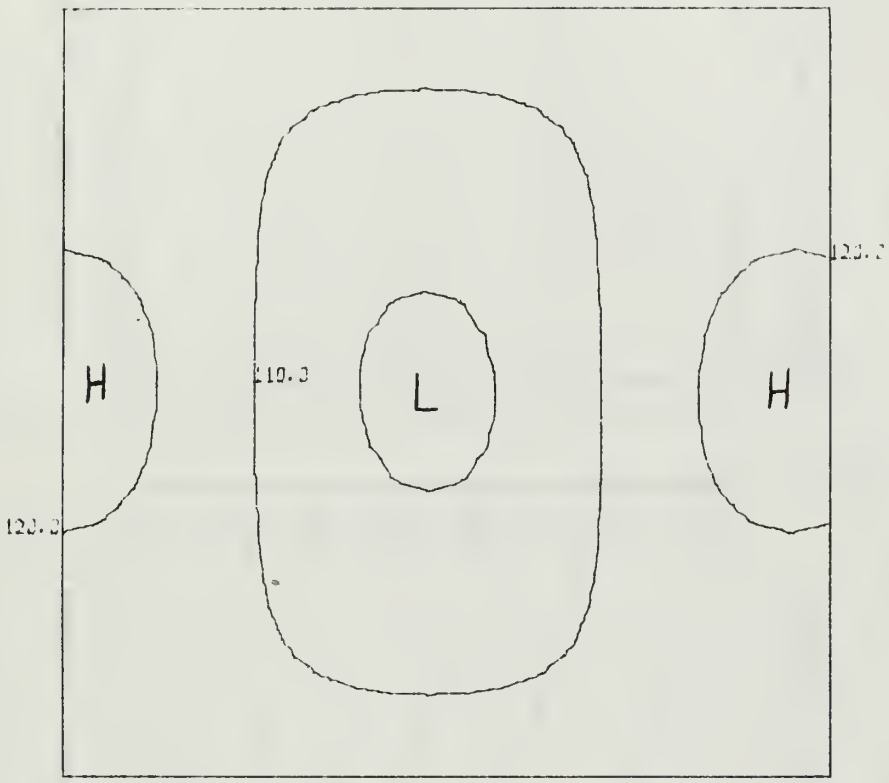


Minimum contour 100 meters, contour interval 10 meters.

Fig. 3. Initial 1000 mb height analysis.

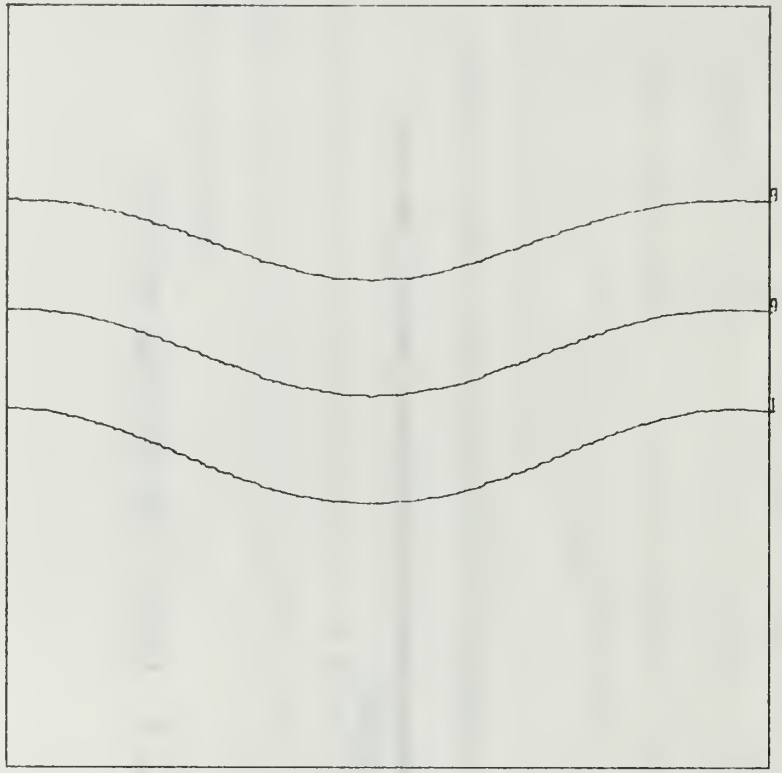

Minimum contour 950 meters, interval 30 meters.

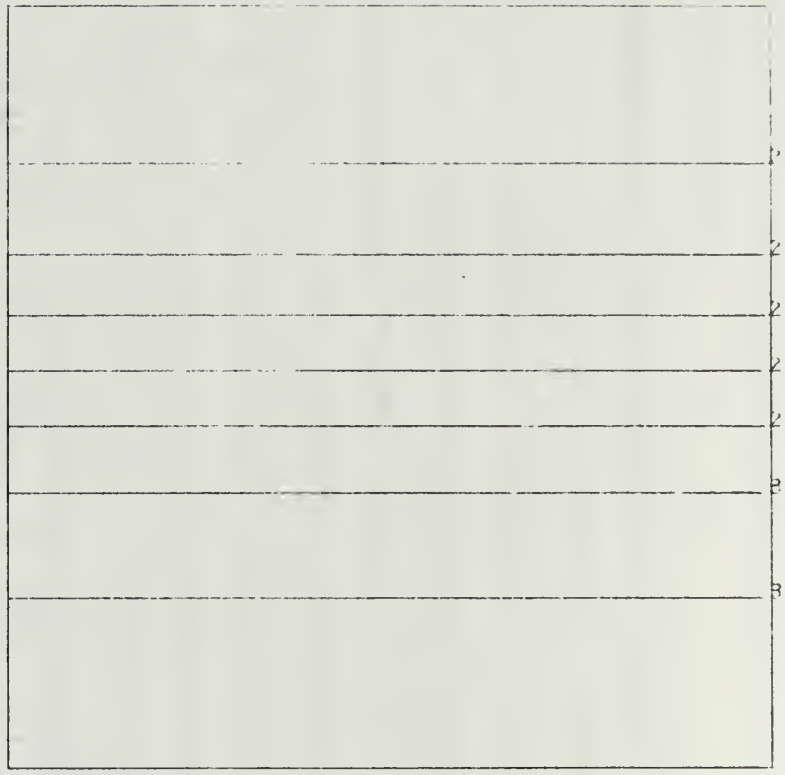

Minimum Isotherm 275°A, interval 5°C.

Fig. 4. Experiment No. 1, initial 900 mb height and potential temperature analysis.

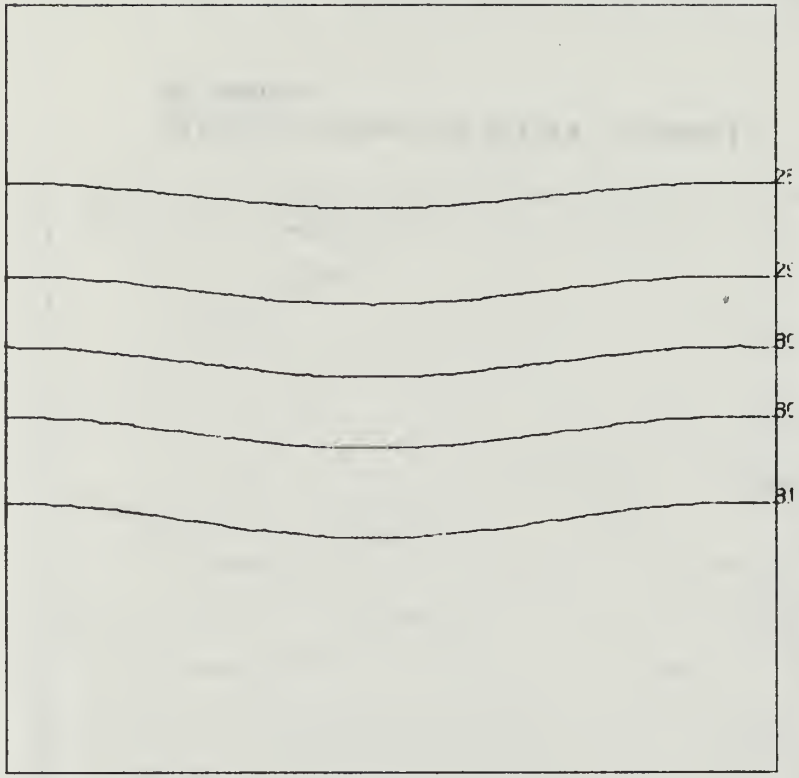

Minimum contour 2880 meters, interval 60 meters.

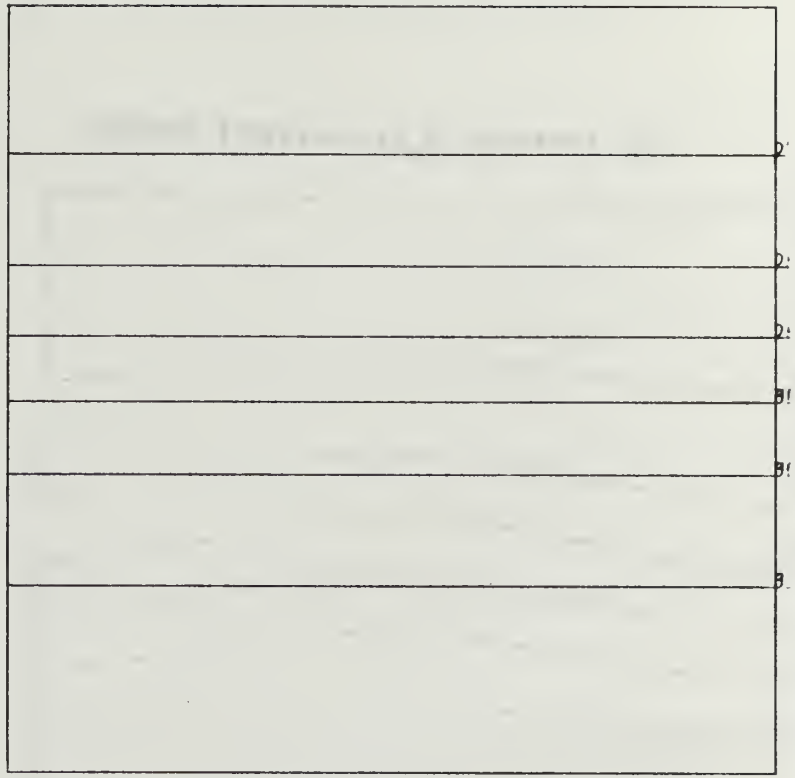

Minimum Isotherm 285°A, interval 5°C.

Fig. 5. Experiment No. 1, initial 700 mb height and potential temperature analysis.

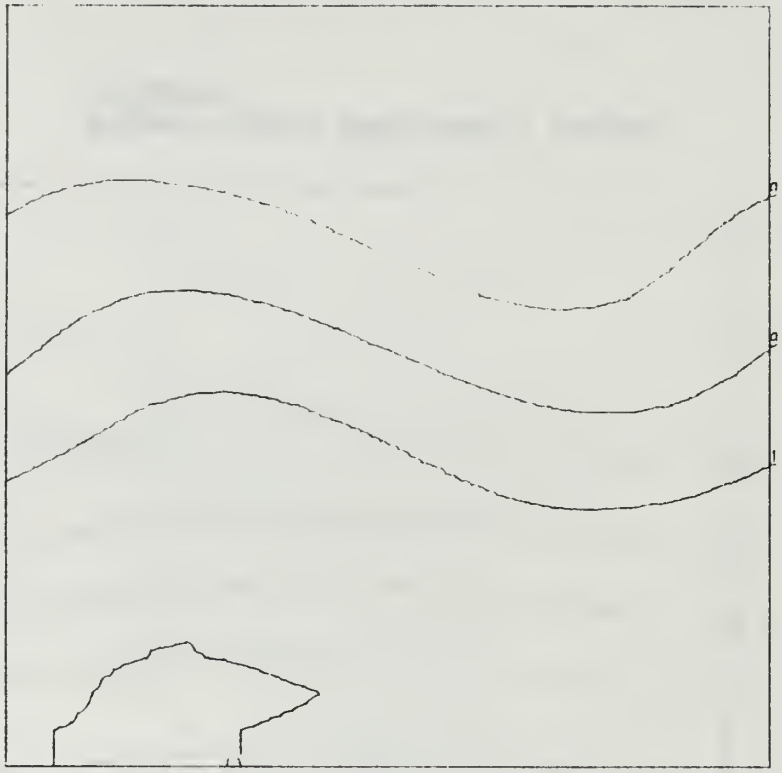

Minimum contour 950 meters, interval 30 meters.

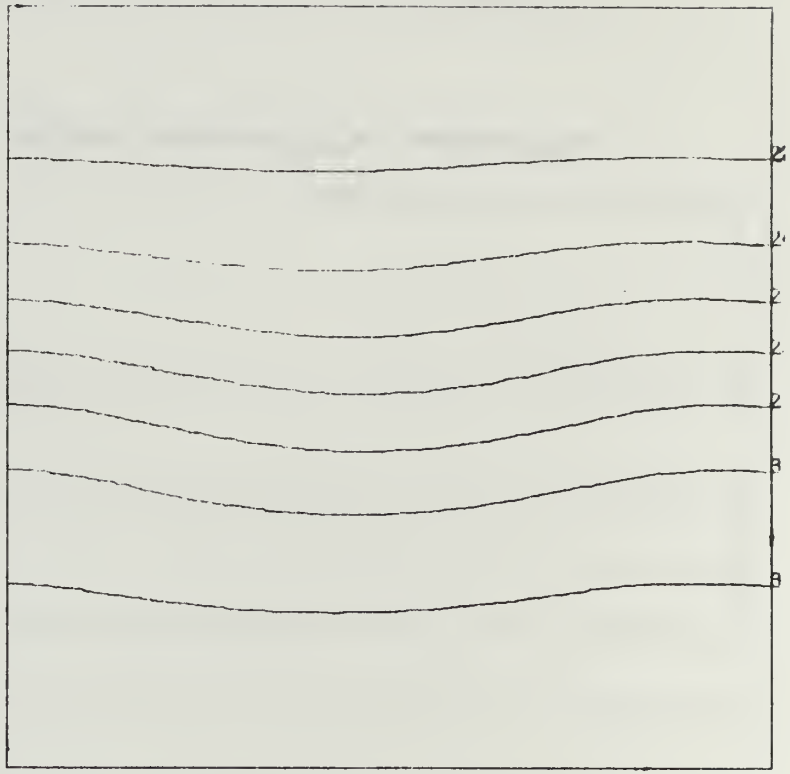

Minimum Isotherm 275°A, interval 5°C.

Fig. 6. Experiment No. 1, 24 Hour 900 mb height and potential temperature analysis.

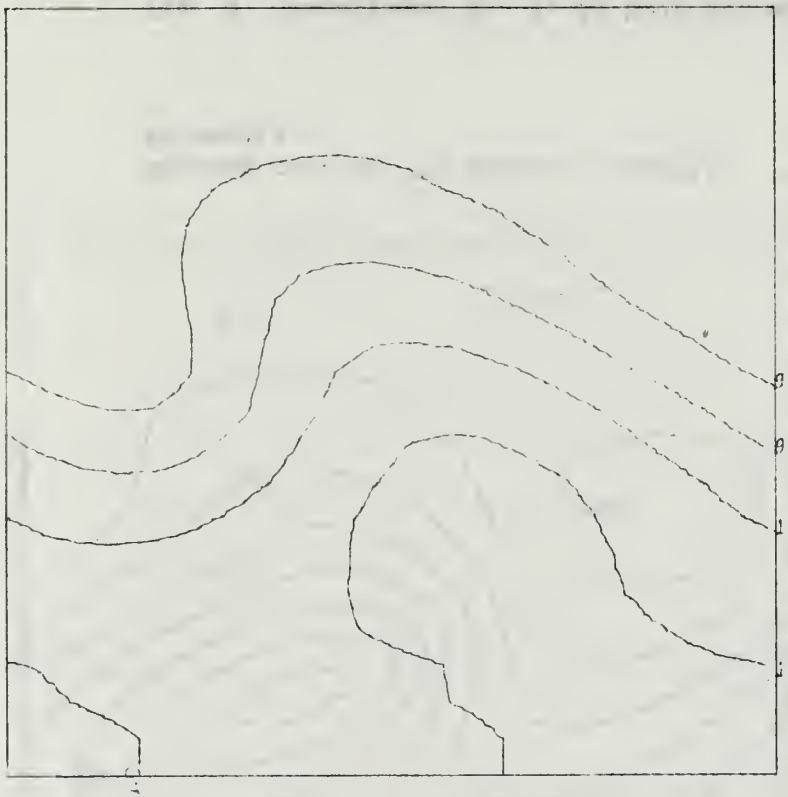

Minimum contour 950 meters, interval 30 meters.

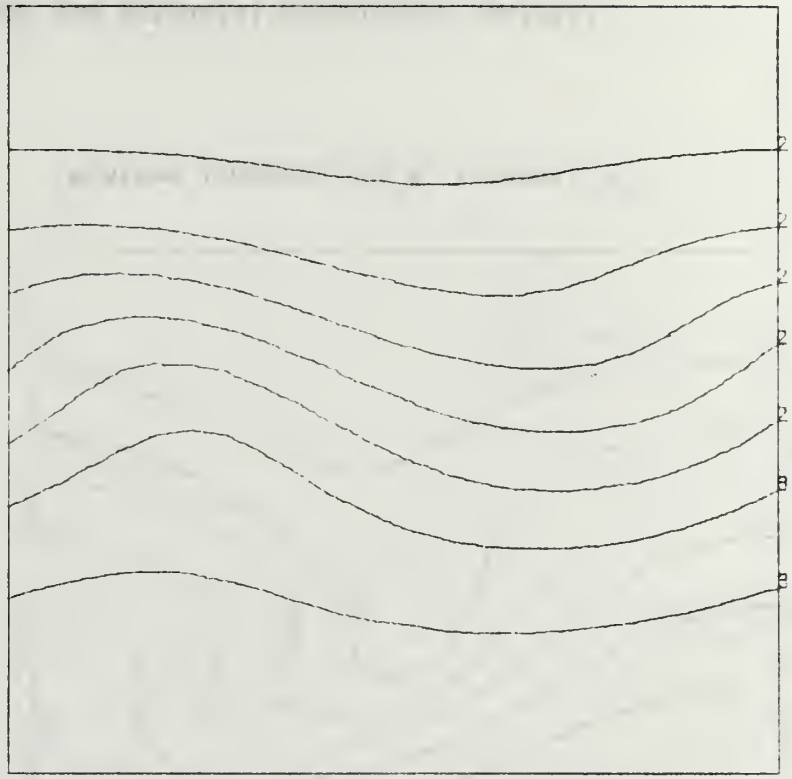

Minimum Isotherm 275°A, interval 5°C.

Fig. 7. Experiment No. 1, 48 Hour 900 mb height and potential temperature analysis.

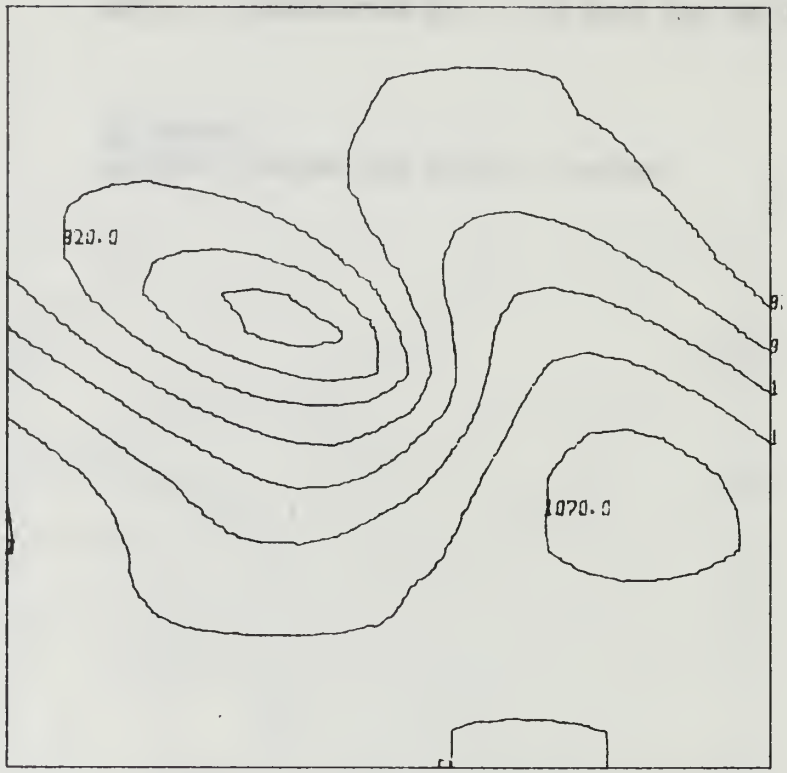


Minimum contour 760 meters, interval 30 meters.

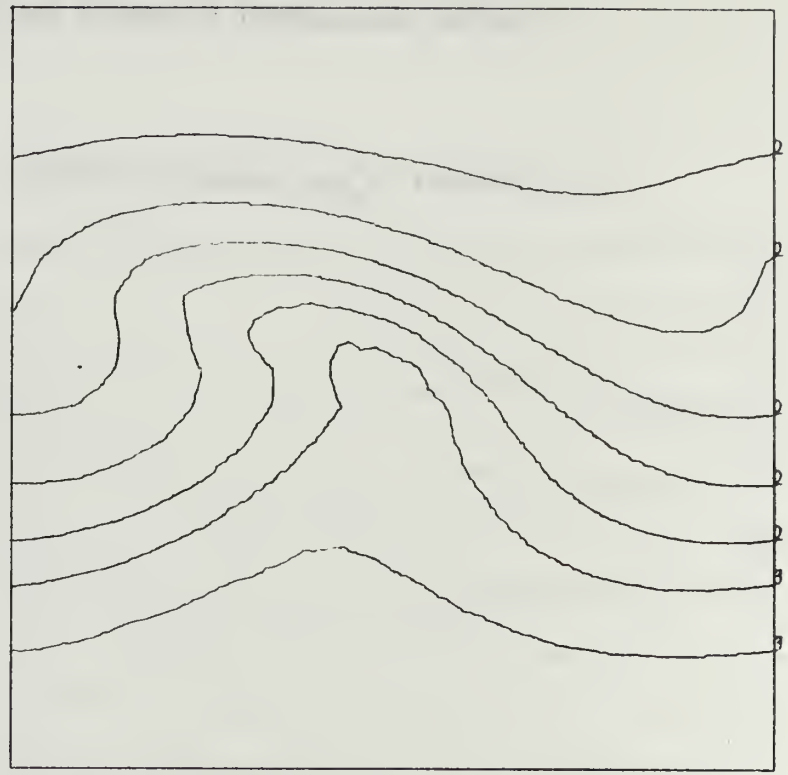

Minimum Isotherm 275°A, interval 5°C.

Fig. 8. Experiment No. 1, 74 Hour 900 mb height and potential temperature analysis.

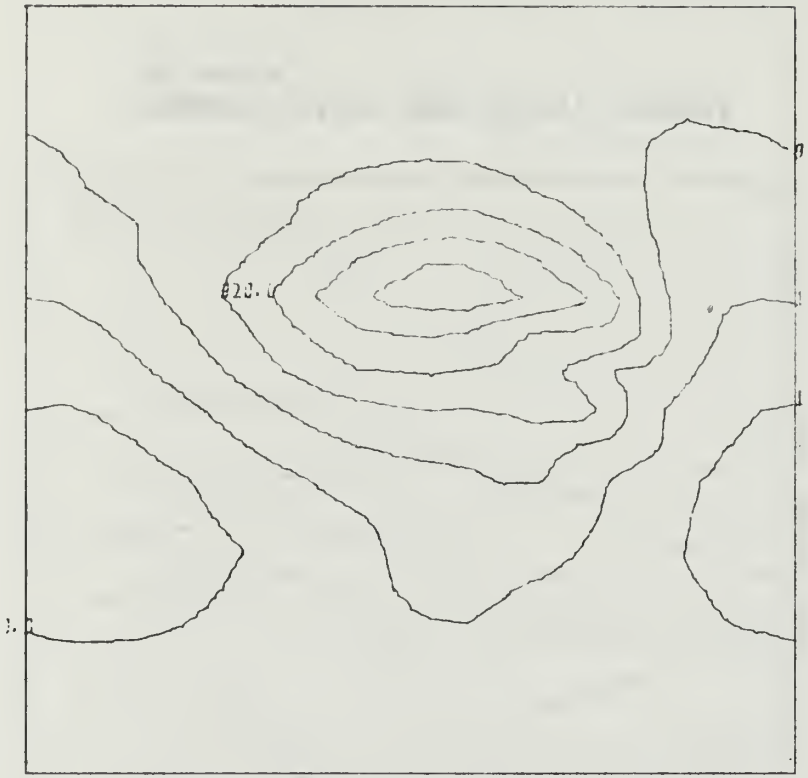

Minimum contour 740 meters, interval 60 meters.

Minimum Isotherm 275°A, interval 5°C.

Fig. 9. Experiment No. 1, 96 Hour 900 mb height and potential temperature analysis.

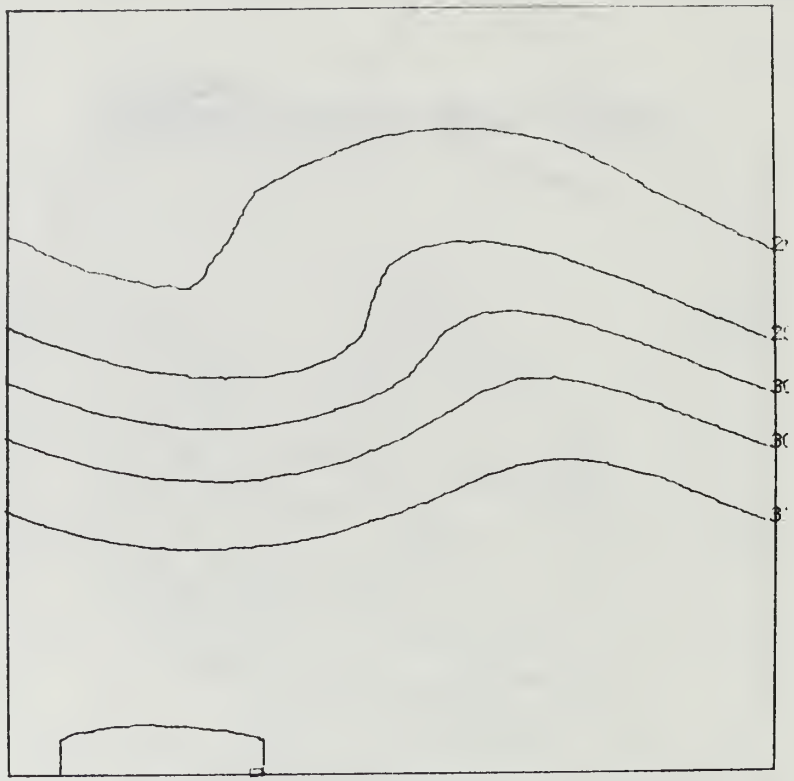

Minimum contour 2880 meters, interval 60 meters.

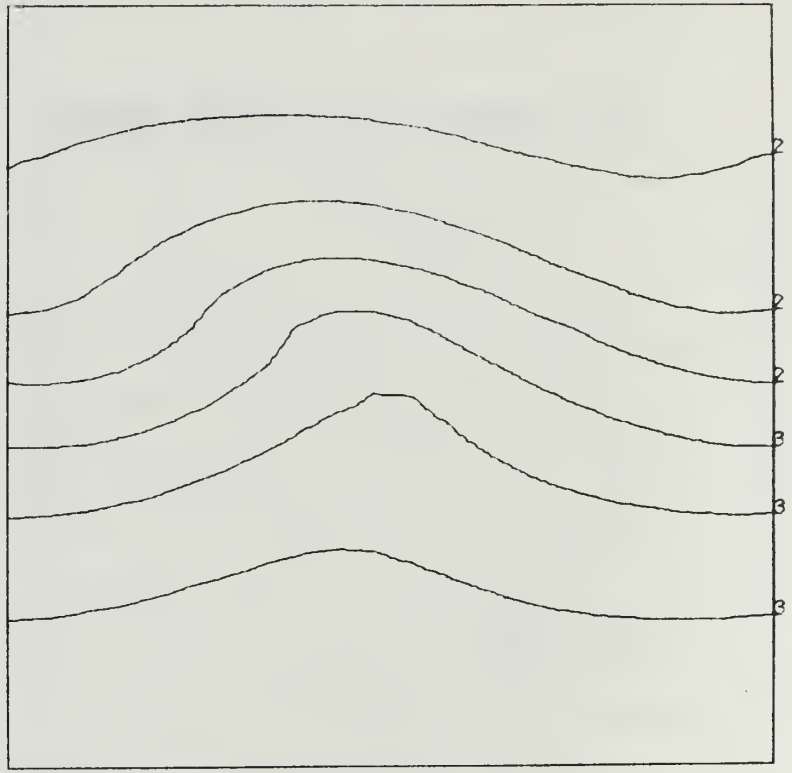

Minimum Isotherm 285°A, interval 5°C.

Fig. 10. Experiment No. 1, 72 Hour 700 mb height and potential temperature analysis.

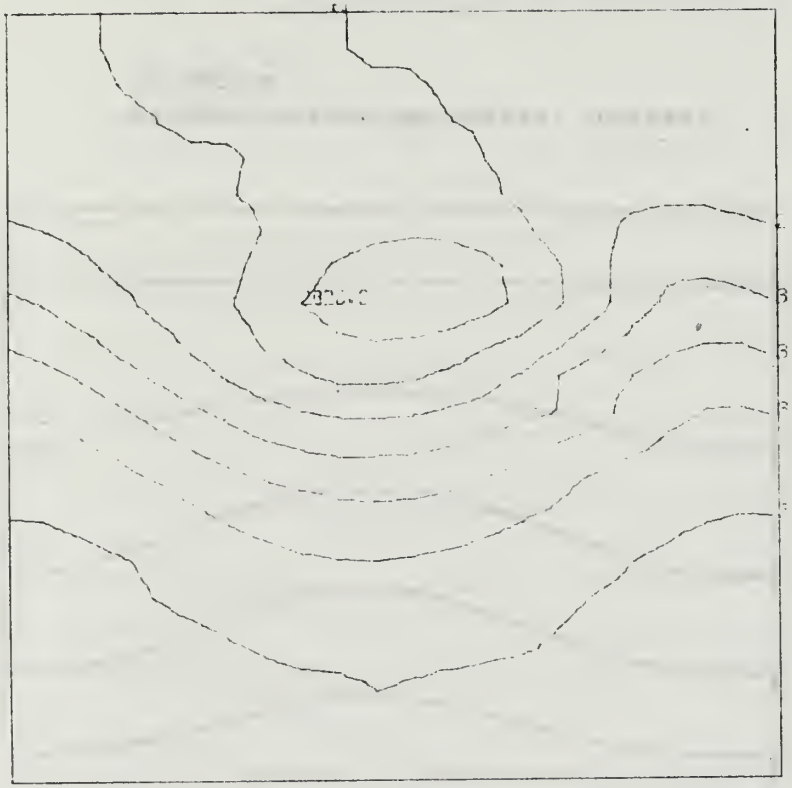

Minimum contour 2820 meters, interval 60 meters.

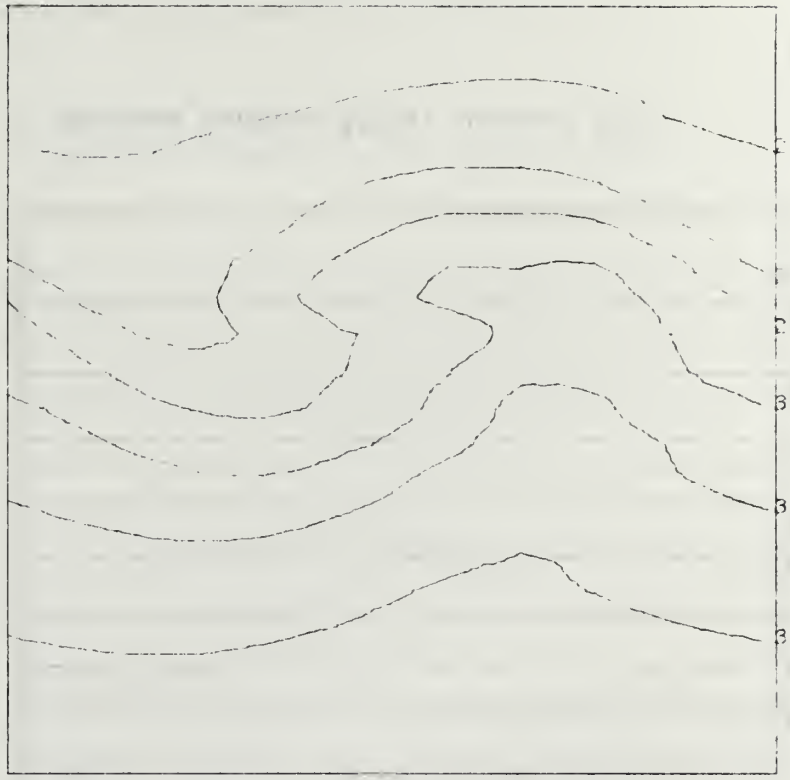

Minimum Isotherm 285°A, interval 5°C.

Fig. 11. Experiment No. 1, 96 Hour 700 mb height and potential temperature analysis.

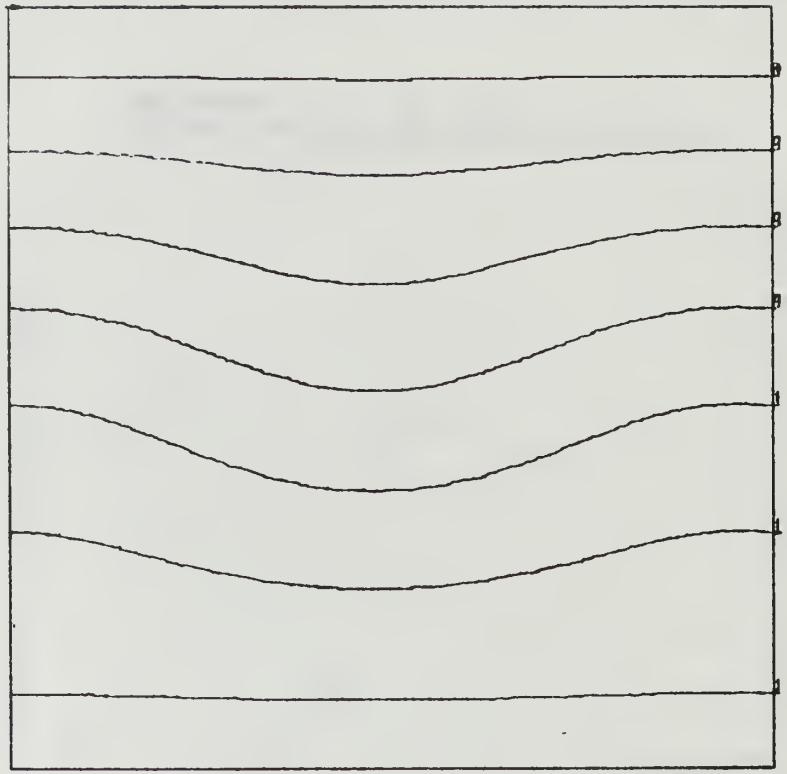

Minimum contour 890 meters, interval 30 meters.

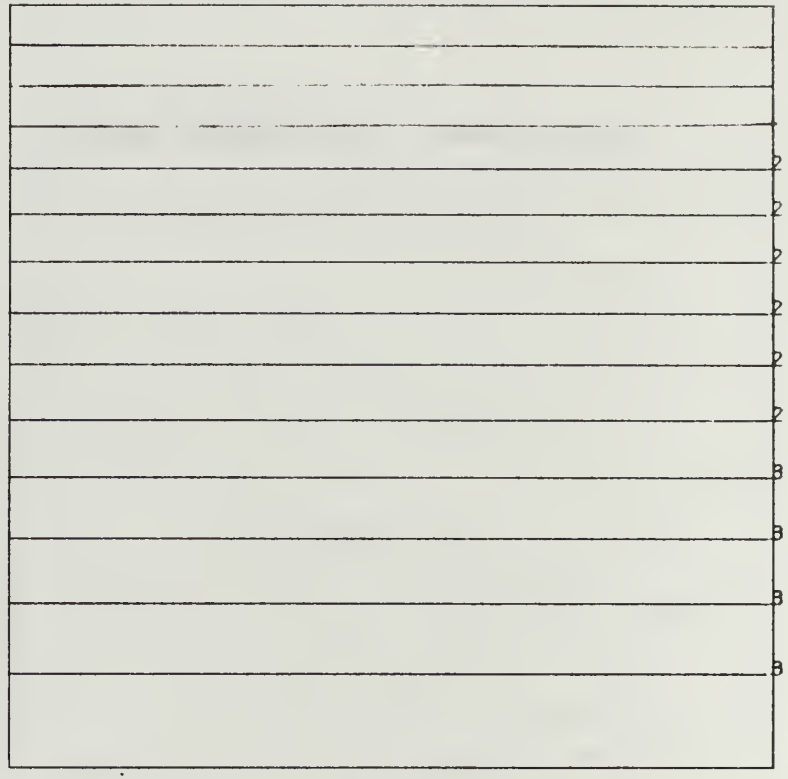

Minimum Isotherm 255°A, interval 5°C.

Fig. 12. Experiment No. 2, Initial 900 mb height and potential temperature analysis.

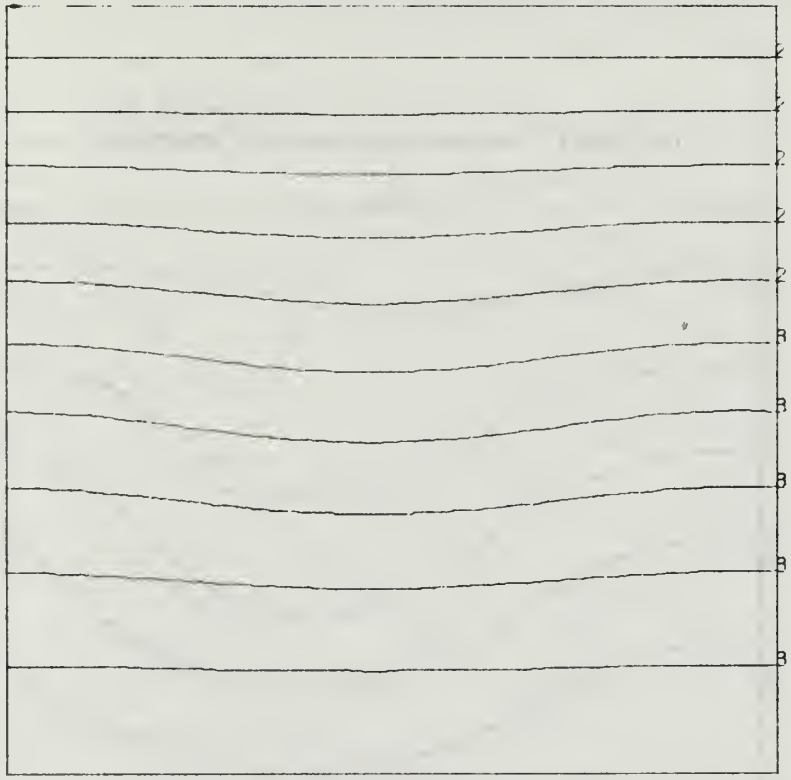

Minimum contour 2700 meters, interval 60 meters.

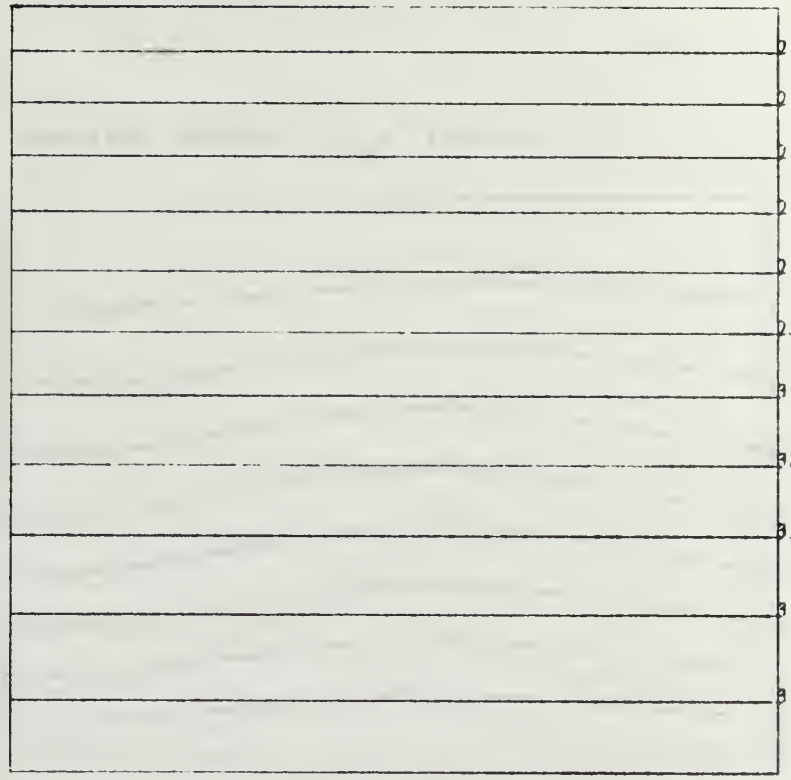

Minimum Isotherm 270°A, interval 5°C.

Fig. 13. Experiment No. 2, Initial 700 mb height and potential temperature analysis.

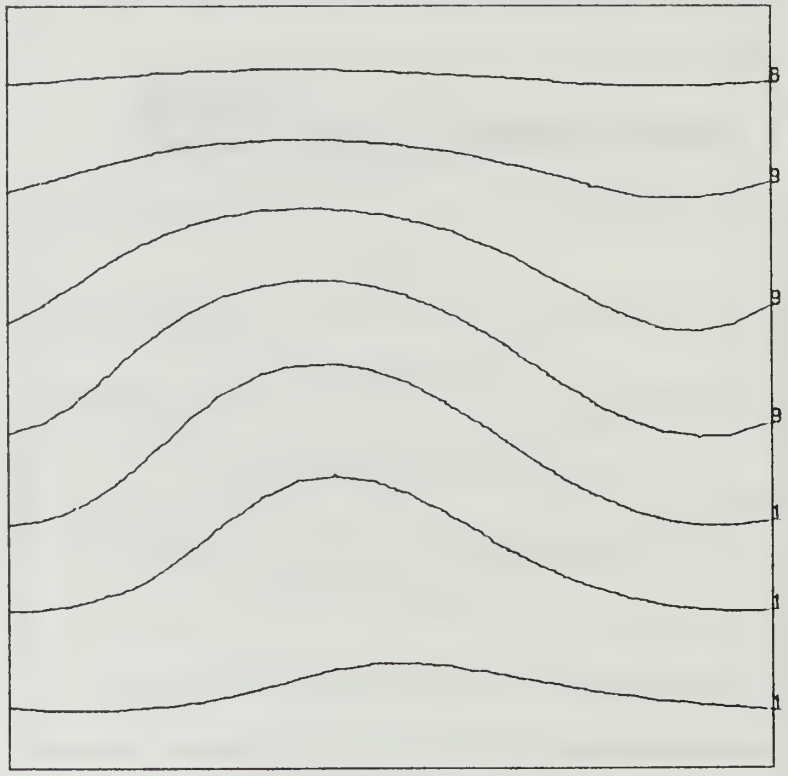

Minimum contour 890 meters, interval 30 meters.

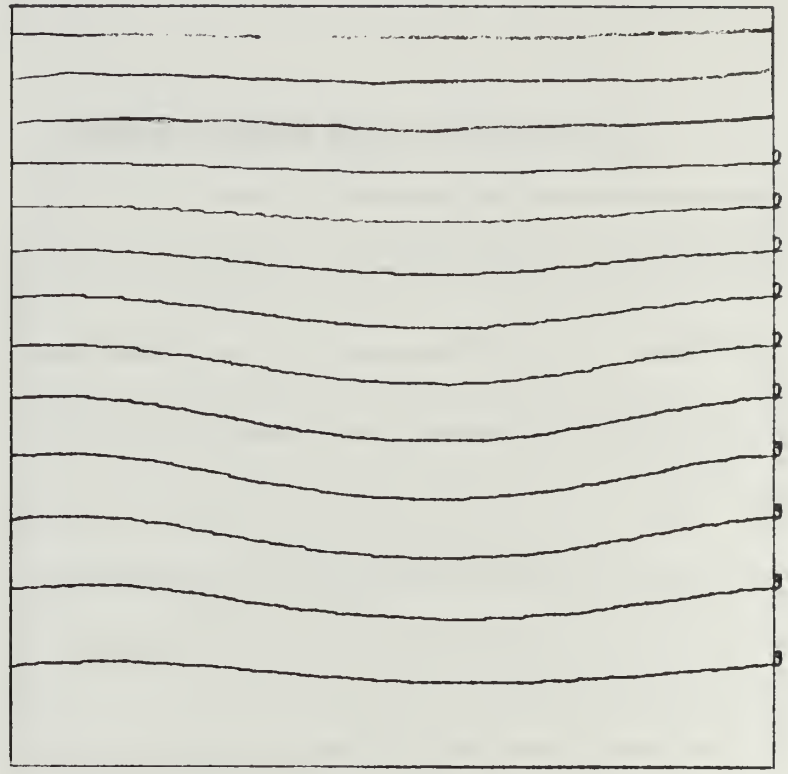

Minimum Isotherm 255°A, interval 5°C.

Fig. 14. Experiment No. 2, 24 Hour 900 mb height and potential temperature analysis.

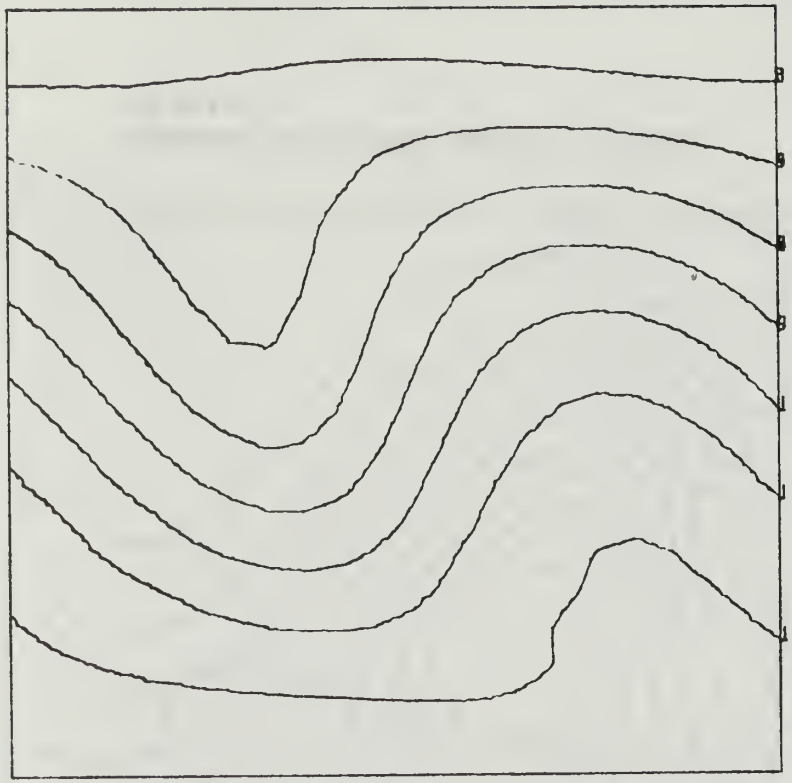

Minimum contour 890 meters, interval 30 meters.

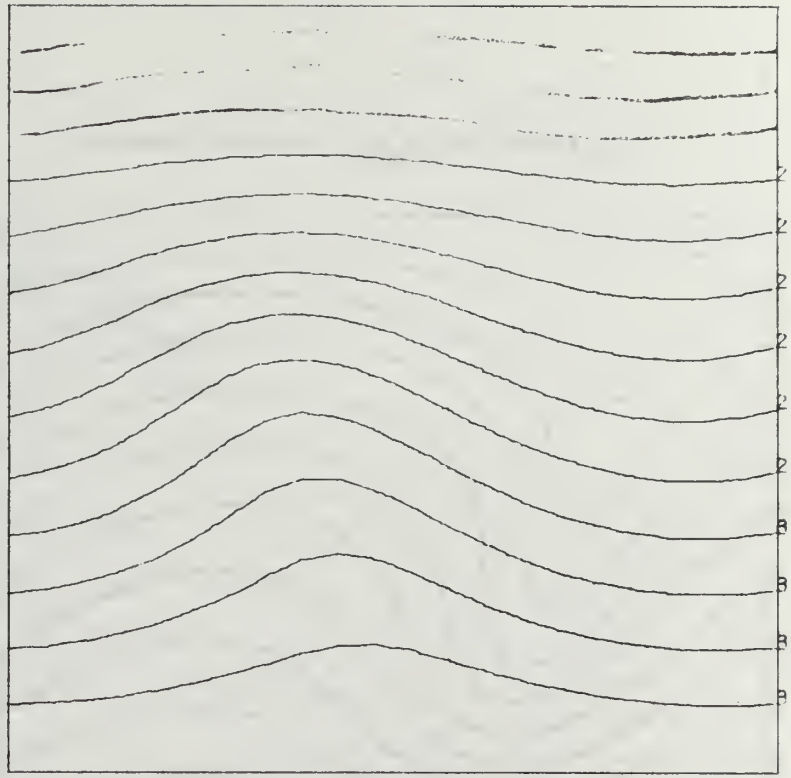

Minimum Isotherm 255°A, interval 5°C.

Fig. 15. Experiment No. 2, 48 Hour 900 mb height and potential temperature analysis.

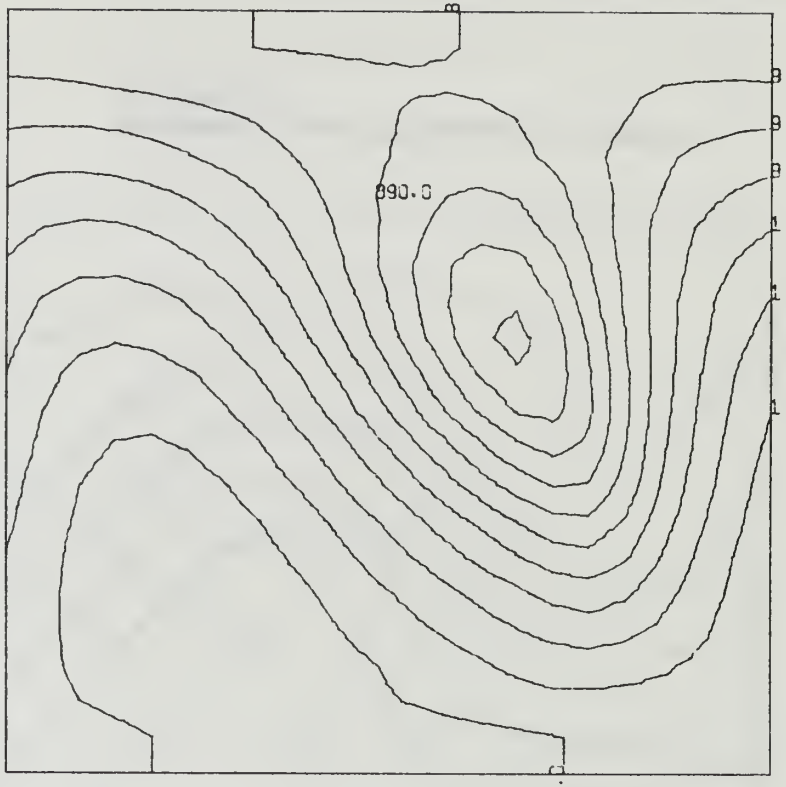

Minimum contour 800 meters, interval 30 meters.

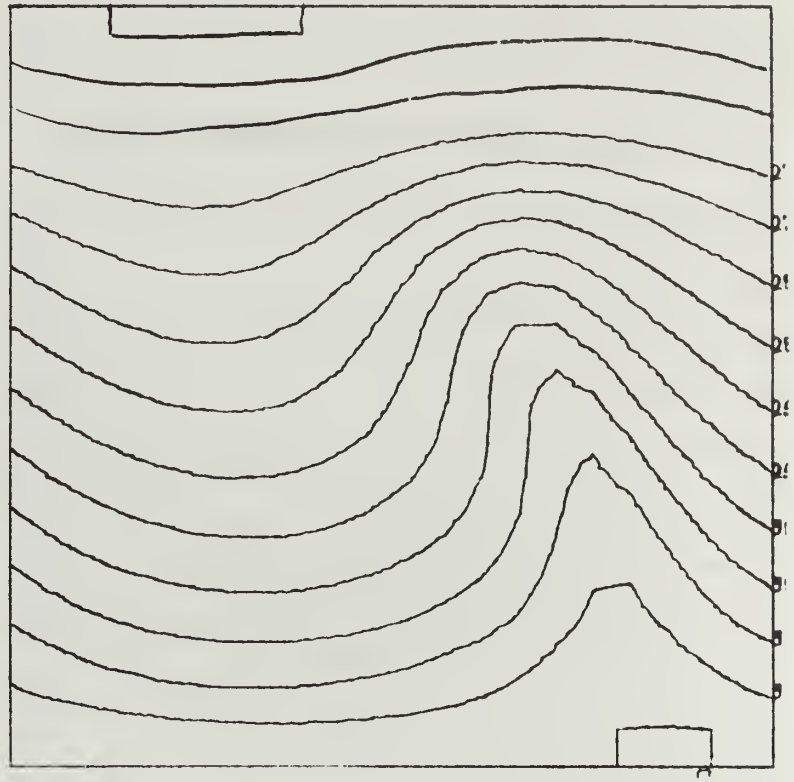

Minimum Isotherm 270°A, interval 5°C.

Fig. 16. Experiment No. 2, 72 Hour 900 mb height and potential temperature analysis.

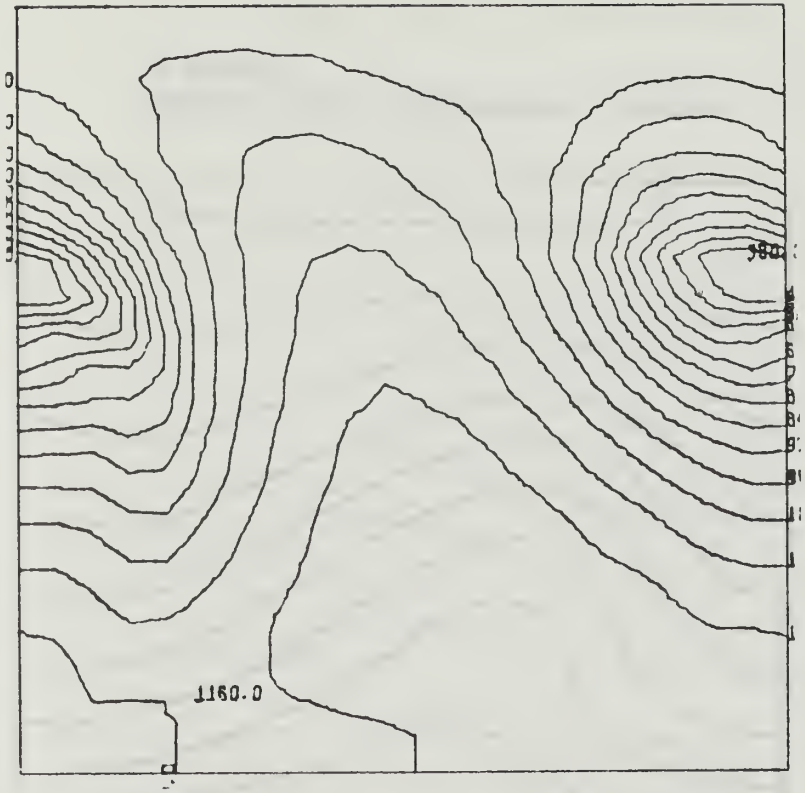


Minimum contour 440 meters, interval 60 meters.

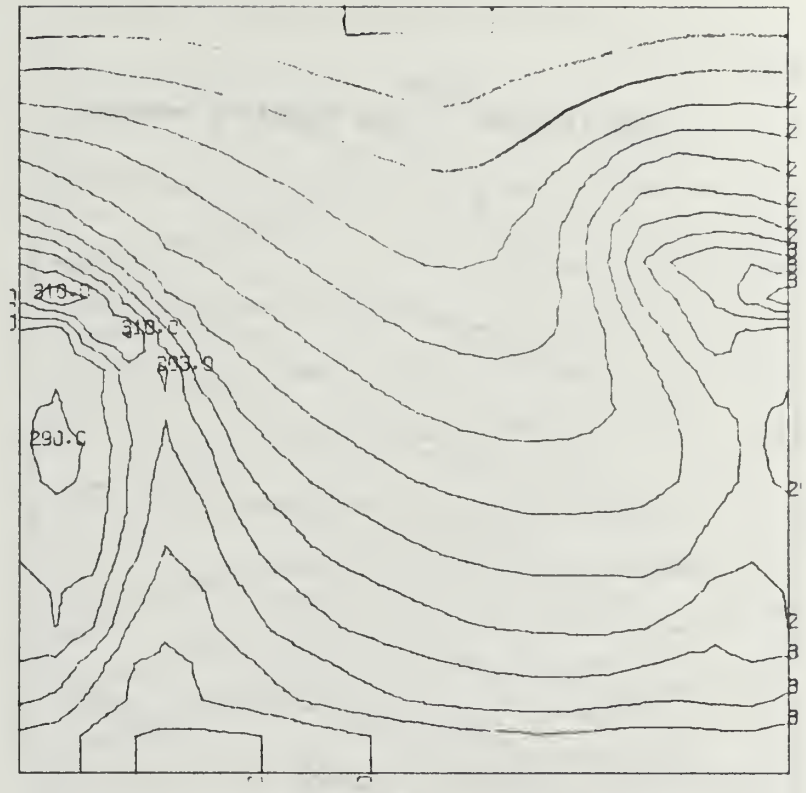


Minimum Isotherm 255°A, interval 5°C.

Fig. 17. Experiment No. 2, 96 Hour 900 mb height and potential temperature analysis.

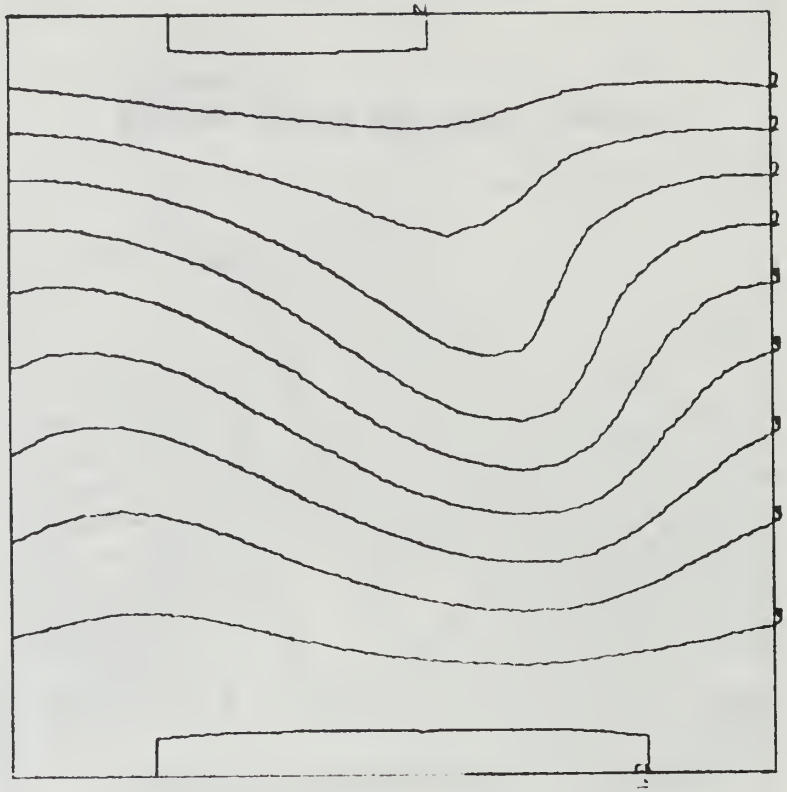

Minimum contour 2700 meters, interval 60 meters.

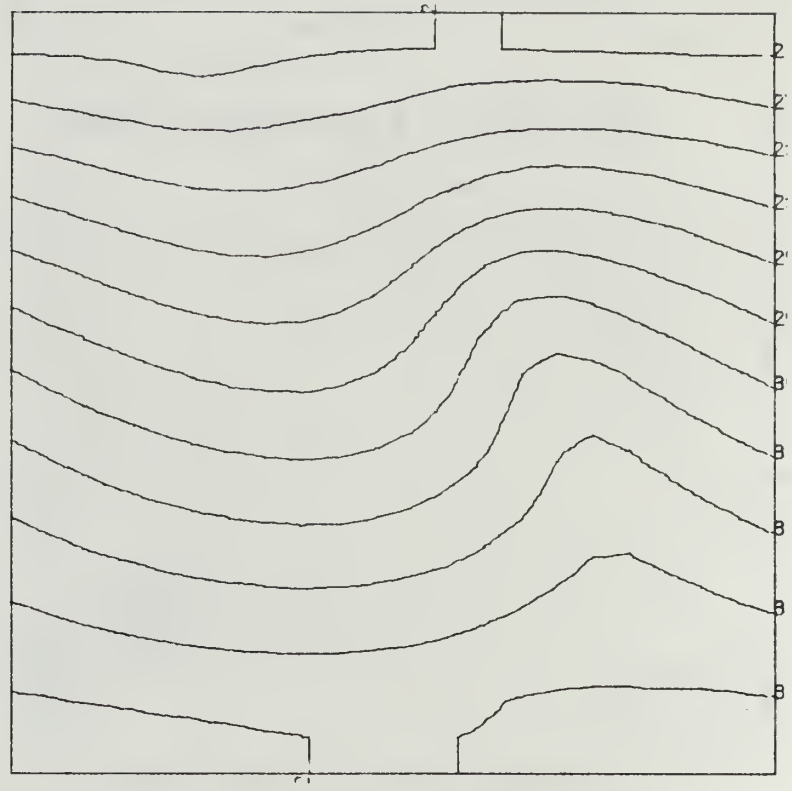

Minimum Isotherm 270°A, interval 5°C.

Fig. 18. Experiment No. 2, 72 Hour 700 mb height and potential temperature analysis.

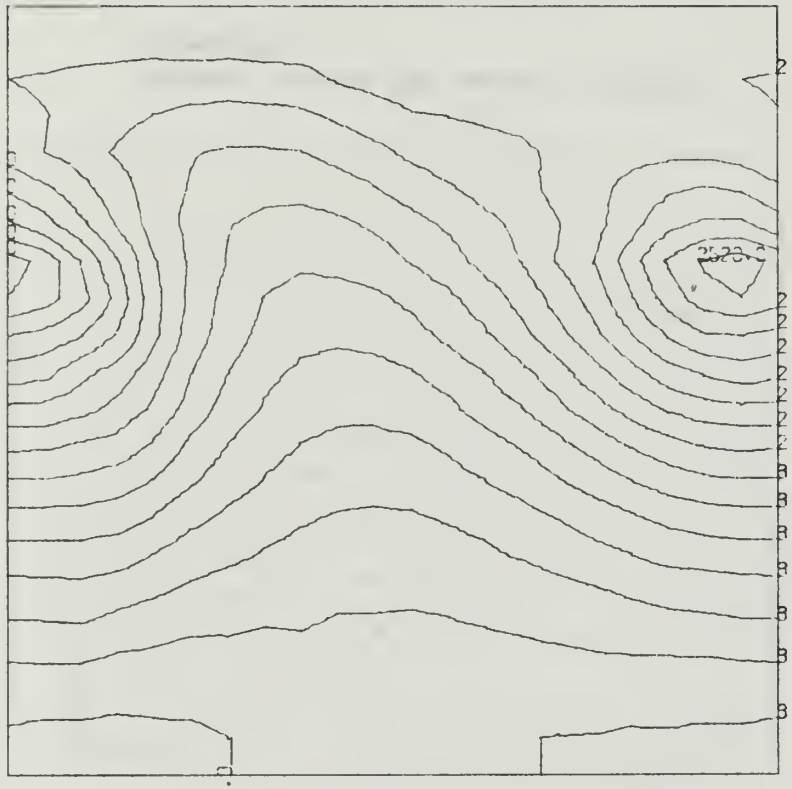

Minimum contour 2520 meters, interval 60 meters.

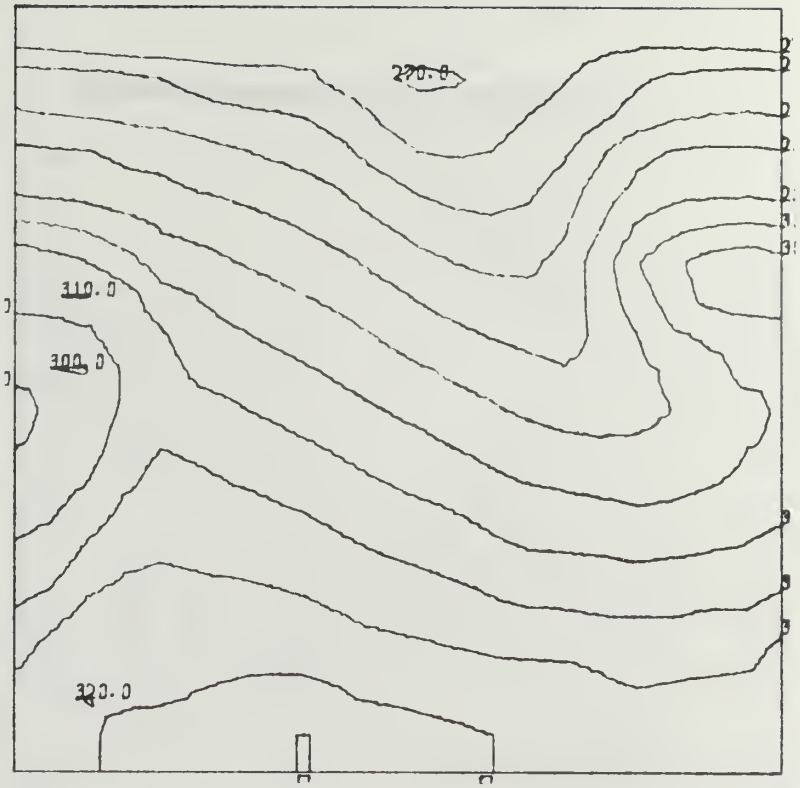


Minimum Isotherm 270°A, interval 5°C.

Fig. 19. Experiment No. 2, 96 Hour 700 mb height and potential temperature analysis.

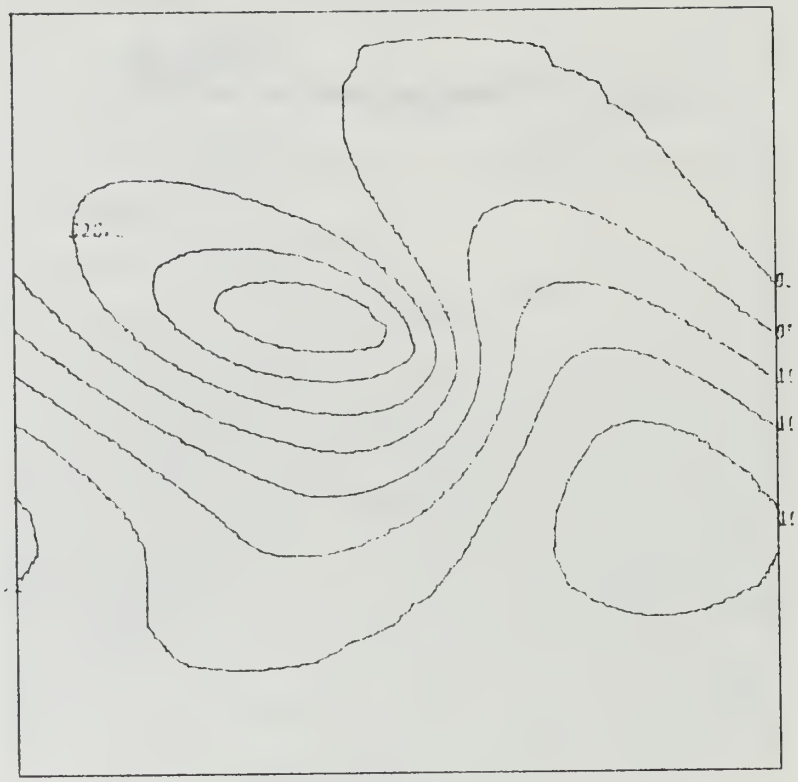

Minimum contour 860 meters, interval 30 meters.

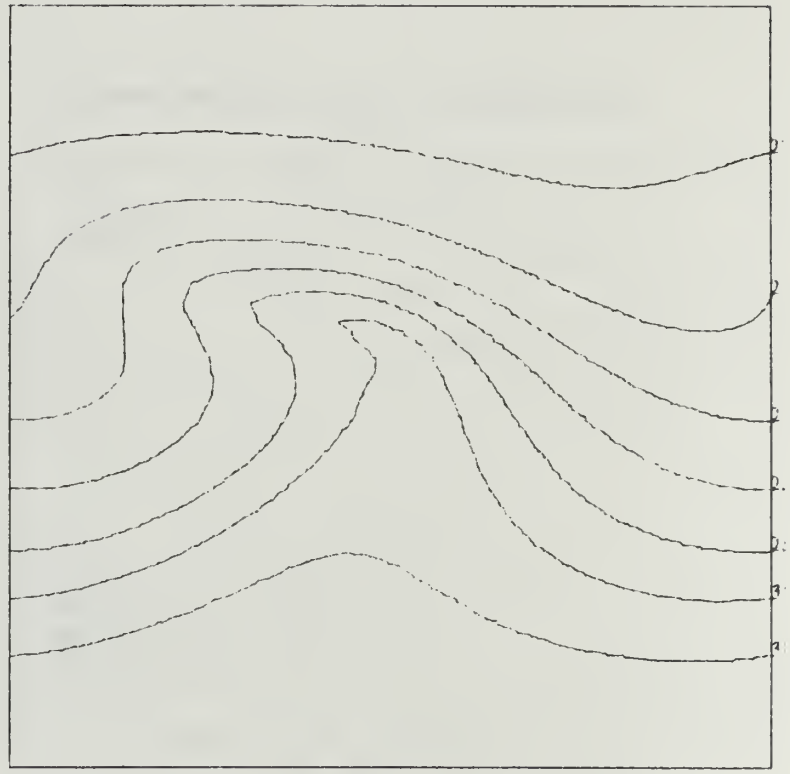

Minimum Isotherm 275°A, interval 5°C.

Fig. 20. Experiment No. 3, 72 Hour 900 mb height and potential temperature analysis.

Minimum contour 680 meters, interval 60 meters.

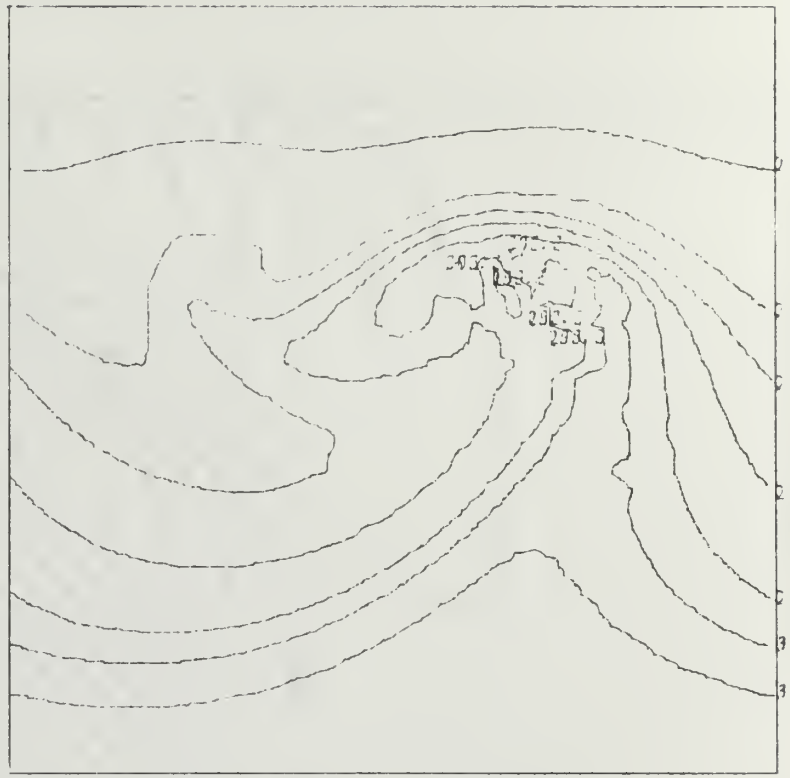

Minimum Isotherm 275°A, interval 5°C.

Fig. 21. Experiment No. 3, 96 Hour 900 mb height and potential temperature analysis.

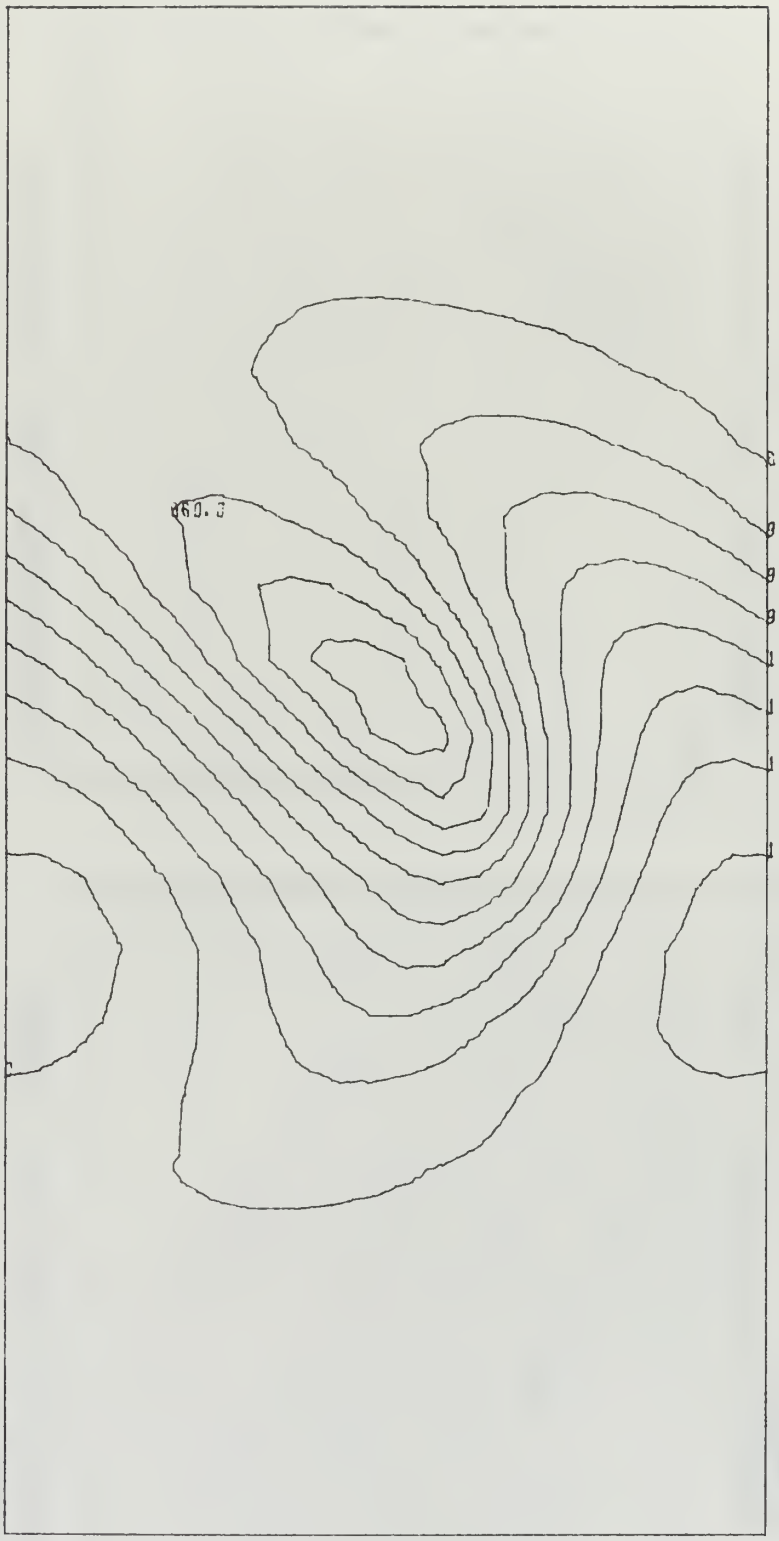

Minimum contour 800 meters, interval 30 meters.

Fig. 22. Experiment No. 7, 72 Hour 900 mb height analysis.

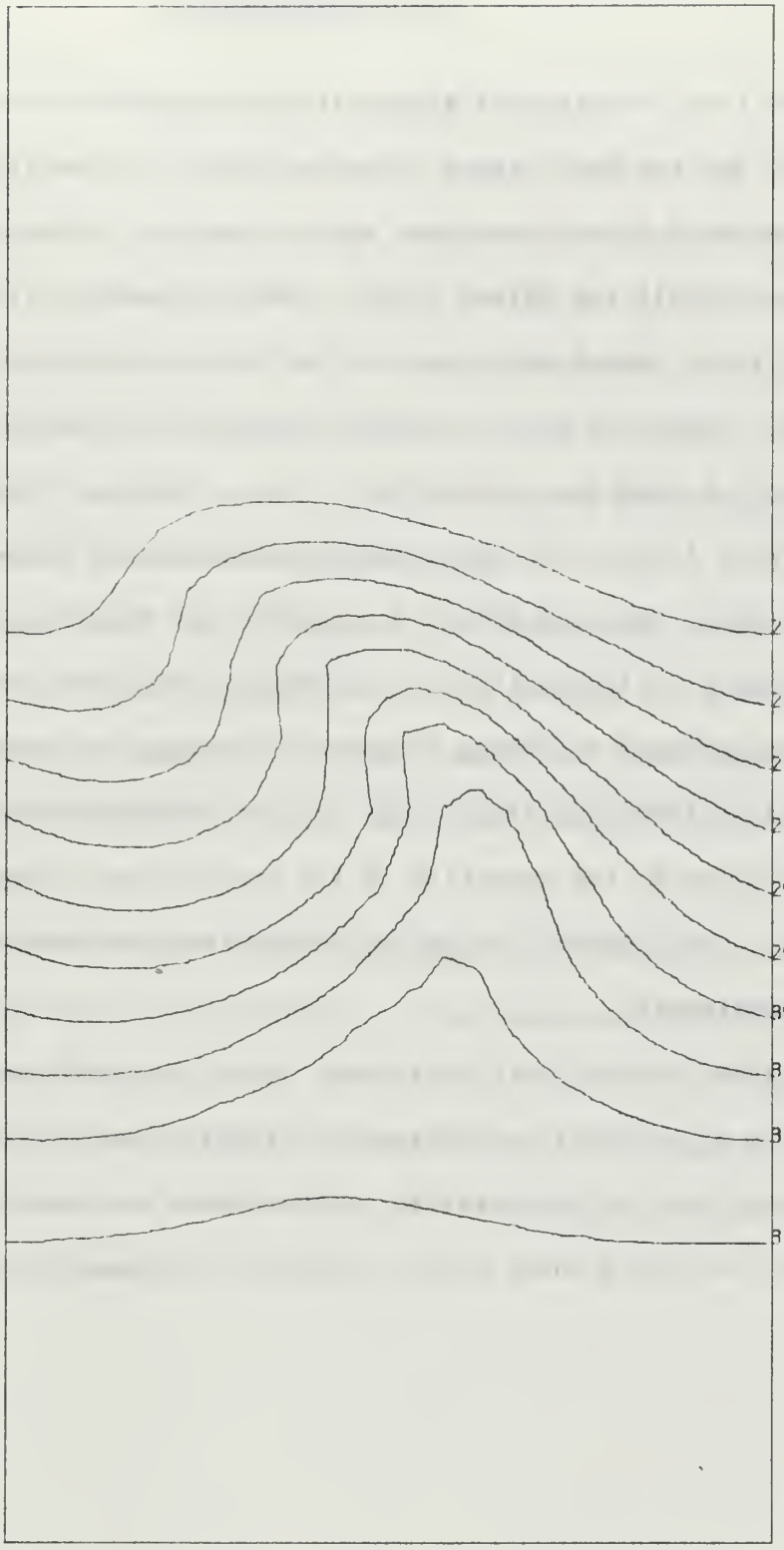

Minimum Isotherm 270°A, interval 5°C.

Fig. 23. Experiment No. 7, 72 Hour 900 mb potential temperature analysis.

## VII. CONCLUSIONS

The time evolution of a baroclinicly unstable disturbance was studied for two basic zonal currents. With horizontal wind shear, cold and warm fronts developed and are similar to the results of Edelmann [1963] and Økland [1969]. With no horizontal wind shear, a cold front formed which was similar to the results of Williams [1969]. This cold front resembled an occluded front at the surface but did not have the life history of an occlusion. In general, the warm front formed from the stretching deformation discussed by Stone [1966] while the cold fronts formed from the shearing deformation discussed by Williams [1967]. In the jet case, the warm front was further enhanced by strong convergence through the action of the vertical deformation field. The lack of frontogenesis at upper levels is explained by the reduction of the vertical wind shear at those levels. The classical occlusion process was not observed in any of the experiments.

Further studies with this model should be conducted with the addition of vertical and horizontal diffusion and with the addition of latent heat of condensation. Other basic currents should be tested, including those with an explicit tropopause.

# APPENDIX A

## EXPERIMENTS WITH BOUNDARY CONDITIONS

Before acceptance of the north-south boundary conditions as specified in Chapter V, various other schemes were tested with limited success. A sample of these schemes with the results follows.

1. The boundary was placed at the outer grid points with the values of all variables determined from a linear extrapolation from the next two interior grid points. The integration became unstable after approximately 120 six-minute time steps.

2. The boundary was again placed at the outer grid points and a special one-sided difference modification was made to the basic diagnostic and prognostic equations. Strong unrealistic wind shear developed along the boundary and the numerical integrations eventually became unstable.

3. Cyclic boundary conditions were applied in the north-south as well as in the east-west directions. The discontinuity in the geopotential field forced the use of a complete wave in both the north-south and east-west directions. This doubled the number of grid points in the domain and made the size of the computer program too large for practical use.

## APPENDIX B

### ENERGY COMPUTATIONS

In pressure coordinates, the total potential energy may be written as

$$EP = \frac{1}{g} \int_A \int_{p_o}^{o} C_p \, T \, dp \, dA, \qquad B.1$$

where "dA" represents an area increment. Now, substituting the definition of potential temperature in (B.1), the expression for the total potential energy becomes,

$$EP = \frac{1}{g} \int_A \int_{p_o}^{o} C_p \, \theta \left(\frac{p}{p_o}\right)^{\kappa} dp \, dA. \qquad B.2$$

In pressure coordinates, the total kinetic energy is written as

$$EK = \frac{1}{2g} \int_A \int_{p_o}^{o} (u^2 + v^2) \, dp \, dA. \qquad B.3$$

## LIST OF REFERENCES


Arakawa, A., 1962: Non-geostrophic effects in the baroclinic prognostic equations. Proc. Intern. Symp. Numerical Weather Prediction, Tokyo, 161-175.

Arakawa, A., 1966: Computational design for long-term numerical integration of the equations of fluid motion: Two-dimensional incompressible flow. Part I. J. Comput. Phys., 1, 119-143.

Bushby, F. H., 1969: Further developments of a model for forecasting rain and weather. Technical Report No. 67 of the Japan Meteorological Agency. II-75-II-84.

Bushby, F. H. and Timpson, M. S., 1967: A 10-level atmospheric model and frontal rain. Quart. J. R. Met. Soc., London, 93, 1-17.

Edelmann, W., 1963: On the behavior of disturbances in a baroclinic channel. Sum. Rept. No. 2, Research in Objective Weather Forecasting, Part F, Contract No. AF61(052)-373, Research Division, Deutscher Wetterdienst, Offenbach, 35 pp.

Gates, W. L., 1960: Static stability measures in the atmosphere. Scientific Rept. No. 3, Dynamical Weather Prediction Project, Department of Meteorology, Univ. of Calif., 22 pp.

Harrison, E. J., 1969: Experiments with a primitive equation model designed for tropical application. M. S. Thesis, Naval Postgraduate School, Monterey, Calif., 60 pp.

Lilly, D. K., 1965: On the computational stability of numerical solutions of time-dependent non-linear geophysical fluid dynamics problems. Mon. Wea. Rev., 93, 11-26.

Lorenz, E. N., 1960: Energy and numerical weather prediction. Tellus, 12, 364-373.

Økland, H., 1969: Experimental integration of a 4-level primitive equation model of the atmosphere. Tellus, 21, 359-367.

Phillips, N. A., 1963: Geostrophic motion. Rev. Geophys., 1, 123-176.

Stone, P. H., 1966: Frontogenesis by horizontal wind deformation fields. J. Atmo. Sci., 23, 455-465.

Stone, P. H., 1969: The meridional structure of baroclinic waves. J. Atmo. Sci., 26, 376-389.

Williams, R. T., 1965: Nonlinear, non-geostrophic effects in a baroclinic atmosphere. J. Atmo. Sci., 22, 388-401.

Williams, R. T., 1967: Atmospheric frontogenesis, a numerical experiment. J. Atmo. Sci., 24, 627-641.

Williams, R. T., and Plotkin, J., 1968: Quasi-geostrophic frontogenesis. J. Atmo. Sci., 25, 201-206.

INITIAL DISTRIBUTION LIST

| | | No. Copies |
|---|---|---|
| 1. | Defense Documentation Center<br>Cameron Station<br>Alexandria, Virginia 22314 | 20 |
| 2. | Library, Code 0212<br>Naval Postgraduate School<br>Monterey, California 93940 | 2 |
| 3. | Naval Weather Service Command<br>Washington Navy Yard<br>Washington, D. C. 20390 | 1 |
| 4. | Dr. Roger T. Williams<br>Department of Meteorology<br>Naval Postgraduate School<br>Monterey, California 93940 | 10 |
| 5. | LCDR Richard R. Hadfield, USN<br>U.S.S. LA SALLE (LPD-3)<br>Fleet Post Office<br>New York, New York 09501 | 2 |
| 6. | Officer in Charge<br>Naval Weather Research Facility<br>Naval Air Station, Building R-48<br>Norfolk, Virginia 23511 | 1 |
| 7. | Commanding Officer<br>Fleet Numerical Weather Central<br>Naval Postgraduate School<br>Monterey, California 93940 | 1 |
| 8. | Director, Naval Research Laboratory<br>Attn: Tech. Services Info. Officer<br>Washington, D. C. 20390 | 1 |
| 9. | Department of Meteorology<br>Code 51<br>Naval Postgraduate School<br>Monterey, California 93940 | 1 |
| 10. | Department of Oceanography<br>Code 58<br>Naval Postgraduate School<br>Monterey, California 93940 | 1 |

No. Copies

11. American Meteorological Society — 1
45 Beacon Street
Boston, Massachusetts 02128

12. Office of Naval Research — 1
Department of the Navy
Washington, D. C. 20360

13. Commander, Air Weather Service — 1
Military Airlift Command
Scott Air Force Base, Illinois 62226

14. AFCRL - Research Library — 1
L. G. Hanscom Field
Attn: Nancy Davis/Stop 29
Bedford, Massachusetts 01730

15. Atmospheric Sciences Library — 1
Environmental Science Services Administration
Silver Spring, Maryland 20910

16. Professor Victor Starr — 1
Department of Meteorology
M. I. T.
Cambridge, Massachusetts 03139

17. Dr. J. Pedlosky — 1
Department of Geophysical Sciences
University of Chicago
Chicago, Illinois 60637

18. Dr. Joanne Simpson — 1
Experimental Meteorology Branch
Environmental Science Services Administration
Coral Gables, Florida 33124

19. National Center for Atmospheric Research — 1
Box 1470
Boulder, Colorado 80302

20. Dr. T. N. Krishnamurti — 1
Department of Meteorology
Florida State University
Tallahassee, Florida 32306

21. Dr. Fred Shuman — 1
Director
National Meteorological Center
Environmental Science Services Administration
Suitland, Maryland 20390

No. Copies

22. Dr. J. Smagorinsky — 1
Director
Geophysical Fluid Dynamics Laboratory
Princeton University
Princeton, New Jersey 08540

23. Professor N. A. Phillips — 1
54-1422
M. I. T.
Cambridge, Massachusetts 02139

24. Professor J. G. Charney — 1
54-1424
M. I. T.
Cambridge, Massachusetts 02139

25. Dr. F. Sanders — 1
Department of Meteorology
M. I. T.
Cambridge, Massachusetts 02139

26. Professor K. Ooyama — 1
Department of Meteorology
New York University
University Heights
New York, New York 10453

27. Dr. M. G. Wurtele — 1
Department of Meteorology
U.C.L.A.
Los Angeles, California 90024

28. Dr. A. Arakawa — 1
Department of Meteorology
U.C.L.A.
Los Angeles, California 90024

29. Dr. W. Edelmann — 1
Research Division
Deutscher Wetterdienst
Offenback am Main
West Germany

30. Dr. J. Holton — 1
Department of Atmospheric Science
University of Washington
Seattle, Washington 98105

No. Copies

31. Mr. Jon Plotkin — 1
Department of Meteorology
M. I. T.
Cambridge, Massachusetts 02139

32. Dr. Michael McIntyre — 1
Department of Applied Mathematics
and Theoretical Physics
Silver Street
Cambridge, England

33. Dr. P. Stone — 1
Harvard University
Cambridge, Massachusetts 02138

34. Dr. J. S. Sawyer — 1
Meteorological Office
Bracknell, England

35. Dr. F. H. Bushby — 1
Meteorological Office
Bracknell, England

36. Professor A. Eliassen — 1
University of Oslo
Oslo, Norway

37. Dr. R. Fjortoft — 1
Meteorological Institute
Oslo, Norway

Security Classification

## DOCUMENT CONTROL DATA - R & D

*(Security classification of title, body of abstract and indexing annotation must be entered when the overall report is classified)*

| 1. ORIGINATING ACTIVITY (Corporate author) | 2a. REPORT SECURITY CLASSIFICATION |
|---|---|
| Naval Postgraduate School<br>Monterey, California 93940 | Unclassified |
| | 2b. GROUP |

3. REPORT TITLE

A Study of Atmospheric Frontogenesis with the Primitive Equations

4. DESCRIPTIVE NOTES *(Type of report and inclusive dates)*

Master's Thesis; April 1970

5. AUTHOR(S) *(First name, middle initial, last name)*

Richard Reuben Hadfield

| 6. REPORT DATE | 7a. TOTAL NO. OF PAGES | 7b. NO. OF REFS |
|---|---|---|
| April 1970 | 56 | 16 |

| 8a. CONTRACT OR GRANT NO. | 9a. ORIGINATOR'S REPORT NUMBER(S) |
|---|---|
| b. PROJECT NO. | |
| c. | 9b. OTHER REPORT NO(S) *(Any other numbers that may be assigned this report)* |
| d. | |

10. DISTRIBUTION STATEMENT

This document has been approved for public release and sale; its distribution is unlimited.

| 11. SUPPLEMENTARY NOTES | 12. SPONSORING MILITARY ACTIVITY |
|---|---|
| | Naval Postgraduate School<br>Monterey, California 93940 |

13. ABSTRACT

The deformation of an unstable baroclinic wave as a result of mean horizontal wind shear is studied with the use of a five-layer primitive equation model. Two basic wind profiles were tested: 1) uniform zonal flow, 2) jet type zonal flow. The jet profile produced a cold front and a warm front, with the warm front being the more intense. The uniform zonal flow produced a cold front. The cold fronts were produced by horizontal shearing deformation fields and the warm front was produced by horizontal stretching deformation fields. The formation of the warm front was also enhanced by strong horizontal convergence. The occlusion process was not observed in the experiments.

DD FORM 1 NOV 65 1473 (PAGE 1)

S/N 0101-807-6811



Security Classification

A-31408

| 14 KEY WORDS | LINK A | | LINK B | | LINK C | |
|---|---|---|---|---|---|---|
| | ROLE | WT | ROLE | WT | ROLE | WT |
| Primitive equation model | | | | | | |
| Frontogenesis | | | | | | |
| Stretching deformation | | | | | | |
| Shearing deformation | | | | | | |

Thesis
H109
c.1
Hadfield
A study of atmospheric frontogenesis with the primitive equations.
118946